Next-Generation Sequencing Reveals Low-Dose Effects of Cationic Dendrimers in Primary Human Bronchial Epithelial Cells

Neus Feliu,[†,§] Pekka Kohonen,[†,§] Jie Ji,[‡] Yuning Zhang,[†] Hanna L. Karlsson,[†] Lena Palmberg,[‡] Andreas Nyström,[†] and Bengt Fadeel*[,†]

[†]Nanosafety & Nanomedicine Laboratory, Division of Molecular Toxicology, and [‡]Division of Lung and Airway Research, Institute of Environmental Medicine, Karolinska Institutet, Stockholm, Sweden. [§]N. Feliu and P. Kohonen contributed equally to this study.

ABSTRACT

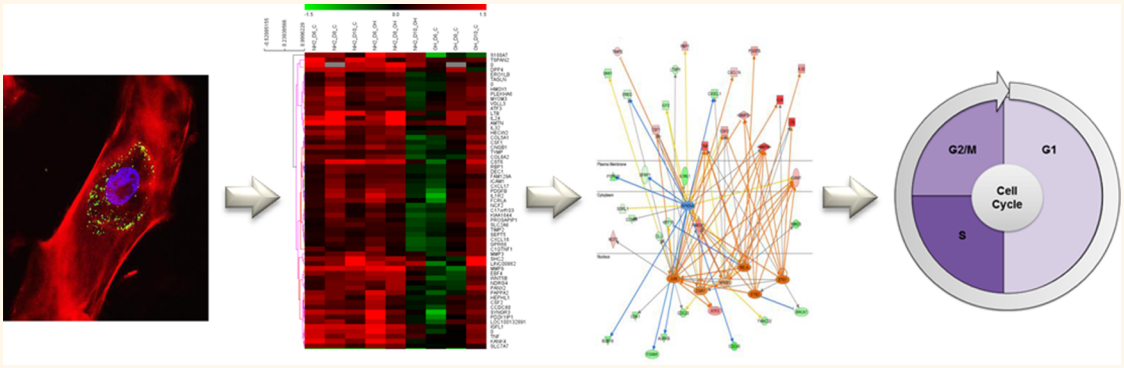

Gene expression profiling has developed rapidly in recent years with the advent of deep sequencing technologies such as RNA sequencing (RNA Seq) and could be harnessed to predict and define mechanisms of toxicity of chemicals and nanomaterials. However, the full potential of these technologies in (nano)toxicology is yet to be realized. Here, we show that systems biology approaches can uncover mechanisms underlying cellular responses to nanomaterials. Using RNA Seq and computational approaches, we found that cationic poly(amidoamine) dendrimers (PAMAM-NH_2) are capable of triggering down-regulation of cell-cycle-related genes in primary human bronchial epithelial cells at doses that do not elicit acute cytotoxicity, as demonstrated using conventional cell viability assays, while gene transcription was not affected by neutral PAMAM-OH dendrimers. The PAMAMs were internalized in an active manner by lung cells and localized mainly in lysosomes; amine-terminated dendrimers were internalized more efficiently when compared to the hydroxyl-terminated dendrimers. Upstream regulator analysis implicated NF-κB as a putative transcriptional regulator, and subsequent cell-based assays confirmed that PAMAM-NH_2 caused NF-κB-dependent cell cycle arrest. However, PAMAM-NH_2 did not affect cell cycle progression in the human A549 adenocarcinoma cell line. These results demonstrate the feasibility of applying systems biology approaches to predict cellular responses to nanomaterials and highlight the importance of using relevant (primary) cell models.

KEYWORDS: poly(amidoamine) dendrimers · next-generation sequencing · systems biology · nanotoxicology

Nanotechnologies offer numerous advantages as therapeutic and diagnostic devices in medicine.[1] However, safety assessment of nanomedicines like all pharmaceuticals is of paramount importance. Understanding the role of physicochemical properties of nanomaterials in determining their biological interactions is not trivial yet remains essential for the safe design of nanomedicines.[2−4] Most nanotoxicological studies published to date have been based on the assessment of acute cytotoxicity, frequently using unrealistically high doses of nanomaterials and more often than not employing transformed cell lines as a model system, rather than primary cells. Furthermore, conventional toxicity assays may not suffice to fully capture the

* Address correspondence to bengt.fadeel@ki.se.

Received for review March 19, 2014 and accepted December 20, 2014.

Published online December 21, 2014
10.1021/nn5061783

complexities of cellular responses toward nanomaterials. Thus, new and more comprehensive approaches are needed.

Global gene expression profiling can be used as a tool to evaluate the interaction between nanomaterials and biological systems.[5] The transcriptomics field has developed rapidly in recent years with the introduction of so-called next-generation sequencing technologies such as RNA sequencing (RNA Seq), which is likely to displace cDNA microarrays as the favored method for gene expression profiling of cells and tissues.[6] RNA Seq probes a multitude of genes and pathways at once, thus providing a useful tool to rapidly identify changes in the expression level of genes following treatment with various compounds. This information, together with other toxicological data, could be used to predict and formulate premises related to mechanisms of toxicity.[7,8] Indeed, the use of global "omics" technologies coupled with appropriate computational approaches to determine statistically significant perturbations of genes or pathways represents an attractive method to identify the potential hazards and mechanisms of action of engineered nanomaterials and points toward a new era of systems toxicology assessment of nanomaterials in accord with the 21st century paradigm of predictive toxicology of chemicals and nanomaterials.[9,10] We and others have previously reported on the use of gene expression profiling to study the impact of nanomaterials, including metal and metal oxide nanoparticles.[11−16] However, few studies have focused on the effects of low doses, or noncytotoxic doses, of nanomaterials on gene expression. Here, we investigated changes in gene expression profiles in primary human bronchial epithelial cells (PBECs) by poly(amidoamine) (PAMAM) dendrimers by using the Hi-Seq 2000/2500 Illumina platform for global RNA sequencing (see Figure S1 for an outline of the approach). Gene Ontology (GO) enrichment analysis and pathway analysis using the Ingenuity Pathway Analysis (IPA) software was performed. In addition, we performed Connectivity Map (CM) analysis[17] to identify putative similarities between the transcriptional signatures of PAMAMs to those induced by other agents. PAMAMs have been widely investigated due to their ease of functionalization and potential biomedical applications and were selected as a small-diameter model nanoparticle because they have very well-defined structures[18] and because previous studies have suggested a correlation between the surface charge of PAMAMs and *in vitro* and *in vivo* responses.[19,20] We therefore evaluated PAMAMs of the same size or generation, with neutral (OH) or positive (NH_2) surface groups (Table S1). Primary human bronchial epithelial cells were selected as a model system, as these cells play an important role in the innate immune defense against inhaled pathogens and particulates.[21] We show that cationic nanoparticles are capable of triggering specific changes in gene expression in primary human lung cells at doses that do not elicit acute cytotoxicity and that these alterations in gene expression are associated with cell cycle arrest. Our study thus demonstrates the feasibility of applying systems biology tools to assess cellular responses to nanomaterials, not least at low doses.

RESULTS

Cationic PAMAMs Are Cytotoxic to Primary Human Bronchial Epithelial Cells. In order to investigate the cytotoxicity of the two dendrimers, (G4) PAMAM-OH and (G4) PAMAM-NH_2, the cell viability of primary bronchial epithelial cells exposed to dendrimers was evaluated. The two nanoparticles have neutral and positive surface charge at physiological pH, based on the pK_a values.[18] We included ZnO nanoparticles as a positive control.[22] The results demonstrated that cell viability of PBECs exposed to PAMAM-OH was slightly decreased only at high doses after 48 h, while, in contrast, PAMAM-NH_2 exhibited pronounced toxicity in a time- and dose-dependent manner, as determined by the LDH assay, which reports a loss of integrity of the plasma membrane (Figure 1A−D). In order to further evaluate the observed cytotoxicity, the Alamar Blue assay was used to assess cell viability following exposure of PBECs to PAMAM-OH and PAMAM-NH_2, and similar results were obtained (Figure S2A−F). Together, the data show that the cationic PAMAMs exhibited stronger toxicity than PAMAMs with neutral surface charge, in line with previous studies of the same class of nanomaterials using other cell models.[19,20] On the basis of these results, we selected a noncytotoxic dose of PAMAM-OH and PAMAM-NH_2 (0.1 μM) for subsequent gene expression profiling studies. This dose corresponds to 1.4215 μg/mL for (G4) PAMAM-NH_2 (MW: 14215 g/mL) and 1.4277 μg/mL for (G4) PAMAM-OH (MW: 14277.1 g/mL)—or about 1.4 μg/mL—which is a relatively low dose when compared to other *in vitro* studies of nanomaterials, where doses ranging from 1 up to 100 or even 200 μg/mL are commonly applied,[23] but still relatively high, should one extrapolate to the *in vivo* situation. Notwithstanding, for the purpose of the present study, a "low" dose is defined as a dose that does not induce acute cytotoxicity in primary human lung cells *ex vivo*.

To further assess the cellular responses to the two dendrimers, we monitored the production of reactive oxygen species (ROS) in PBECs exposed to PAMAM-OH and PAMAM-NH_2, using the CM-H_2DCFDA assay. *tert*-Butyl hydroperoxide was used as a positive control. The data showed that PAMAMs at doses from 0.01 to 10 μM did not trigger ROS production in PBECs up to 5 h (Figure S3A,B). At 48 h, both PAMAMs triggered an increase in ROS compared to the control (not shown).

PAMAMs Are Taken up by Bronchial Epithelial Cells and Are Localized in Lysosomes. Despite their small size,

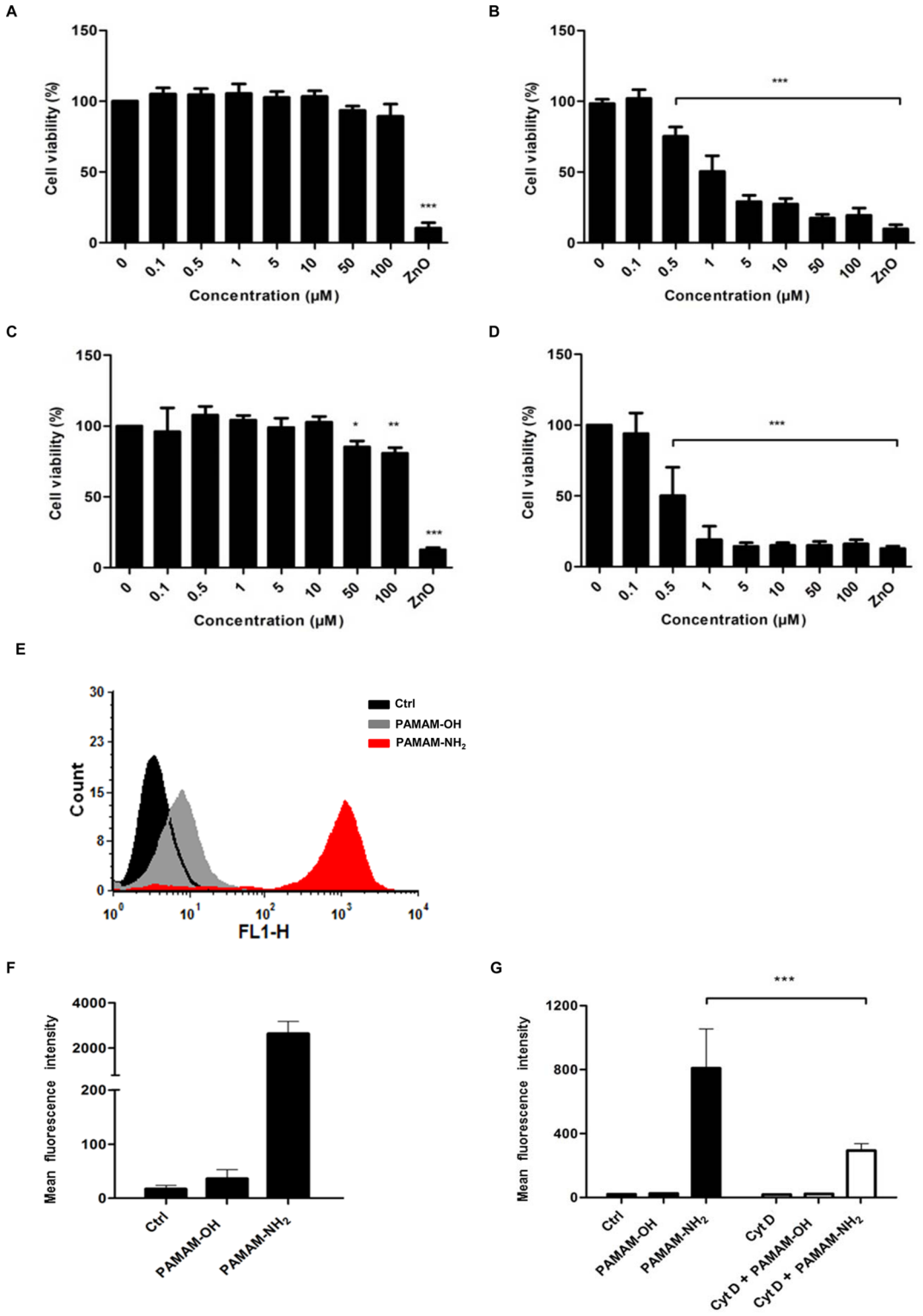

Figure 1. Cationic PAMAMs trigger dose- and time-dependent cytotoxicity in primary human bronchial epithelial cells. PBECs were exposed to PAMAM-OH for 24 h (A) and 48 h (C) and to PAMAM-NH_2 for 24 h (B) and 48 h (D), and cell viability was measured using the LDH assay. ZnO nanoparticles (100 μg/mL) were included as a positive control. Results are shown as mean values $\pm$ SD using cells from three independent human donors (*$p < 0.001$). (E, F) Uptake of fluorescence-labeled PAMAMs (0.1 μM) at 24 h as measured by flow cytometry. (G) Uptake of PAMAMs by PBECs at 4 h of exposure in the presence or absence of cytochalasin D (5 μg/mL). Results shown as mean values $\pm$ SD using cells from 3 to 4 independent donors (***$p < 0.001$).**

dendrimers are reported to be internalized into cells by endocytosis; however, depending on the surface functionality, differences in uptake mechanisms may exist.[24] Here we studied the internalization of PAMAM dendrimers in primary human lung cells (PBECs). To this end, PAMAM-OH and PAMAM-NH_2 were labeled

with fluorescent groups (fluorescein derivates), as previously reported.[25,26] The fluorescence labeling imposed little or no changes on the hydrodynamic size or zeta potential of the PAMAM-NH_2 or PAMAM-OH dendrimers (Table S1). Furthermore, because of inherent limitations in determining the properties of low-generation PAMAMs using such techniques, FT-IR measurements were also performed and confirmed that the behavior of the two PAMAMs was very similar before and after modification (Figure S4A,B). As shown in Figure 1E,F, PAMAM-NH_2 appeared to be more efficiently internalized compared with PAMAM-OH. Fluorescence spectrometry analysis indicated that the fluorescence intensity of PAMAM-NH_2 was 2.7-fold higher than for PAMAM-OH and that the number of dye molecules per PAMAM was 0.53 and 0.69 for PAMAM-OH and PAMAM-NH_2, respectively. However, the differences in brightness do not explain the marked differences in cellular uptake between the two dendrimers, and we therefore attributed this to differences in the surface charge of the PAMAMs (see Table S1). Furthermore, our results indicated that PAMAM-NH_2 were internalized through an actin cytoskeleton-dependent process since a significant decrease of cellular internalization was observed following pretreatment of PBECs with cytochalasin D (Figure 1G). Previous studies using various cell lines have shown that dendrimers are internalized by both clathrin-dependent endocytosis and macropinocytosis and are eventually delivered to the lysosomal compartment.[27] Using confocal microscopy we found that PAMAMs are located in lysosomes, as demonstrated by colocalization of the labeled PAMAMs with LysoTracker-stained organelles, but we found no evidence of nuclear localization (Figure S5A). To further elucidate the subcellular localization of the two PAMAMs, we performed confocal microscopy of PBECs exposed to fluorescently labeled PAMAM dendrimers for 48 h and costained the cells with antibodies to lysosome-associated membrane protein-1 (LAMP-1). These data confirmed the lysosomal localization of the PAMAM-NH_2 dendrimers and a mostly lysosomal localization of the PAMAM-OH dendrimers as well (Figure 2C).

Since cellular uptake of PAMAM-OH was very low (at 0.1 μM), we also determined uptake of PAMAM-OH at higher doses (up to 10 μM) at 24 and 48 h in order to evaluate the ability of PBECs to internalize these nanoparticles. The data showed time- and dose-dependent uptake of PAMAM-OH; notably, at the administered dose of 10 μM, the cellular internalization of PAMAM-OH appeared to be equal to that of PAMAM-NH_2 given at a dose of 0.1 μM, as evidenced by flow cytometry-based quantification of cellular uptake (Figure 2A,B). These results were supported by confocal microscopy based imaging of cellular uptake at different doses (Figure S5B).

Noncytotoxic Doses of PAMAM-NH_2 Induce Changes in Gene Expression in Lung Cells. Next, the levels of transcripts affected in PBECs following exposure to the two different PAMAMs were investigated using RNA sequencing technology. To this end, PBECs obtained from three different human donors were exposed to PAMAM-OH (0.1 μM), PAMAM-NH_2 (0.1 μM), or medium alone for 48 h. The RNA sequencing generated ~10.2 Gb of raw sequence data. The filtered data set comprised approximately 333 million 50 bp reads that were distributed almost evenly between the nine analyzed samples (Table S2), yielding a very high sequencing depth (30−40 million reads per sample). More than 80% of the obtained reads could map to the annotated human genome (GRCh37). Data normalization was carried out in conjunction with the count-based differential expression analysis using R/Bioconductor.[28] Differential tag abundance using counts of genes, filtered to include only tags with an abundance of above 1 count per million (cpm), was determined using the R/Bioconductor package edgeR and the negative binomial model[29] as described in Materials and Methods. Gene-wise statistical tests were conducted and revealed that PAMAM-OH did not elicit any transcriptional responses, whereas PAMAM-NH_2 exerted specific transcriptional effects leading to increased expression of 61 genes and decreased expression of 152 genes (Figure 3A,B), after filtering for donor-specific effects. Of these, 52 and 145, respectively, could be annotated with a gene symbol. The heat map shown in Figure 3C of the induced and suppressed transcripts of PAMAM-NH_2-exposed samples relative to matched controls and PAMAM-OH exposures illustrates the agreement of results from different donors in terms of the fold-change values and the lack thereof in the case of PAMAM-OH-exposed samples.

GO Enrichment Analysis Reveals up- and down-Regulated Categories of Genes. In order to better understand and classify the transcriptional changes observed in cells exposed to PAMAM-NH_2, Gene Ontology enrichment analysis using the R/Bioconductor topGO packages was undertaken. Notably, the GO category for "cell division" encompassing 47/152 genes ($p < 10^{-22}$) was the most strongly down-regulated category, and the checkpoint kinase-encoding gene, BUB1, the gene coding for the marker of proliferation Ki-67 (MKI67), and the tyrosine phosphatase-encoding gene CDC25C were among the most affected genes in this category (Table S3). Gene categories related to regulation of cell cycle checkpoints were also altered, including the highly conserved MCM10, MCM3, and MCM4 genes encoding mini-chromosome maintenance (MCM) proteins that are involved in the initiation of eukaryotic genome replication.[30] Genes coding for proteins responsible for the G2/M transition of the mitotic cell cycle such as the cyclin B1 (CCNB1) are needed to promote the entrance into mitosis (M phase) by

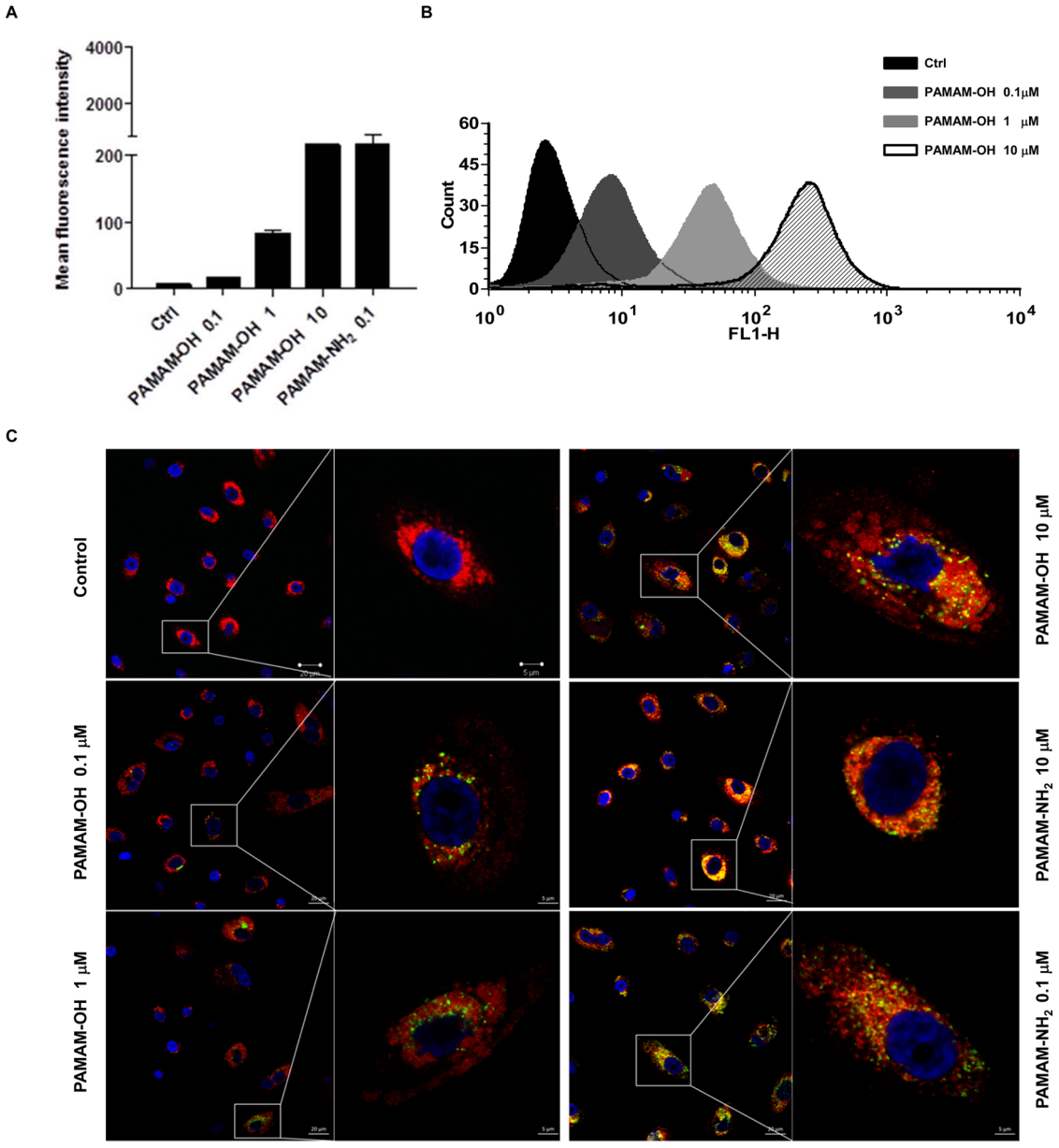

Figure 2. Cellular internalization of PAMAM dendrimers by primary human bronchial epithelial cells. (A) Uptake of fluorescence-labeled PAMAM-OH dendrimers at various concentrations *vs* PAMAM-NH2 dendrimers (0.1 μM) at 48 h as measured by flow cytometry. Results shown as mean values $\pm$ SD using cells from 3 independent donors. (B) Representative histograms. (C) Lysosomal localization of PAMAM dendrimers in PBECs. Uptake of PAMAM-OH and PAMAM-NH_2 at 48 h, as observed by confocal microscopy. PBECs were exposed to the indicated concentrations of PAMAMs (green) and costained with LAMP-1 (red) and DAPI (blue).

phosphorylating multiple proteins, including the FOXM1 cell cycle transcriptional activator.[31] The DNA topoisomerase 2-α (TOP2A) is an enzyme that controls and alters the topologic states of DNA during DNA transcription and replication.[32] BIRC5 (also known as survivin), a member of the inhibitor of apoptosis (IAP) gene family possessing pro-mitotic as well as antiapoptotic functions,[33] was also found among the top down-regulated categories (Table S3). In sum, GO analysis of the RNA Seq data derived from PBECs exposed to PAMAM-NH_2 revealed that all of the most significantly down-regulated gene categories are related to cell division or cell cycle regulation.

The strongest effects were thus seen for the down-regulated genes; however, GO categories with *increased* activities included extracellular matrix disassembly, positive regulation of cell migration, and immune responses (Table S3). Hence, the matrix metalloproteinases, MMP9 and MMP3, involved in degradation of the extracellular matrix, were up-regulated, along with TIMP2, a natural inhibitor of the matrix metalloproteinases, which has a unique role among TIMP family members in its ability to also directly suppress the proliferation of endothelial cells.[34] WNT5B, a member of the WNT gene family, was also found among the most up-regulated genes.

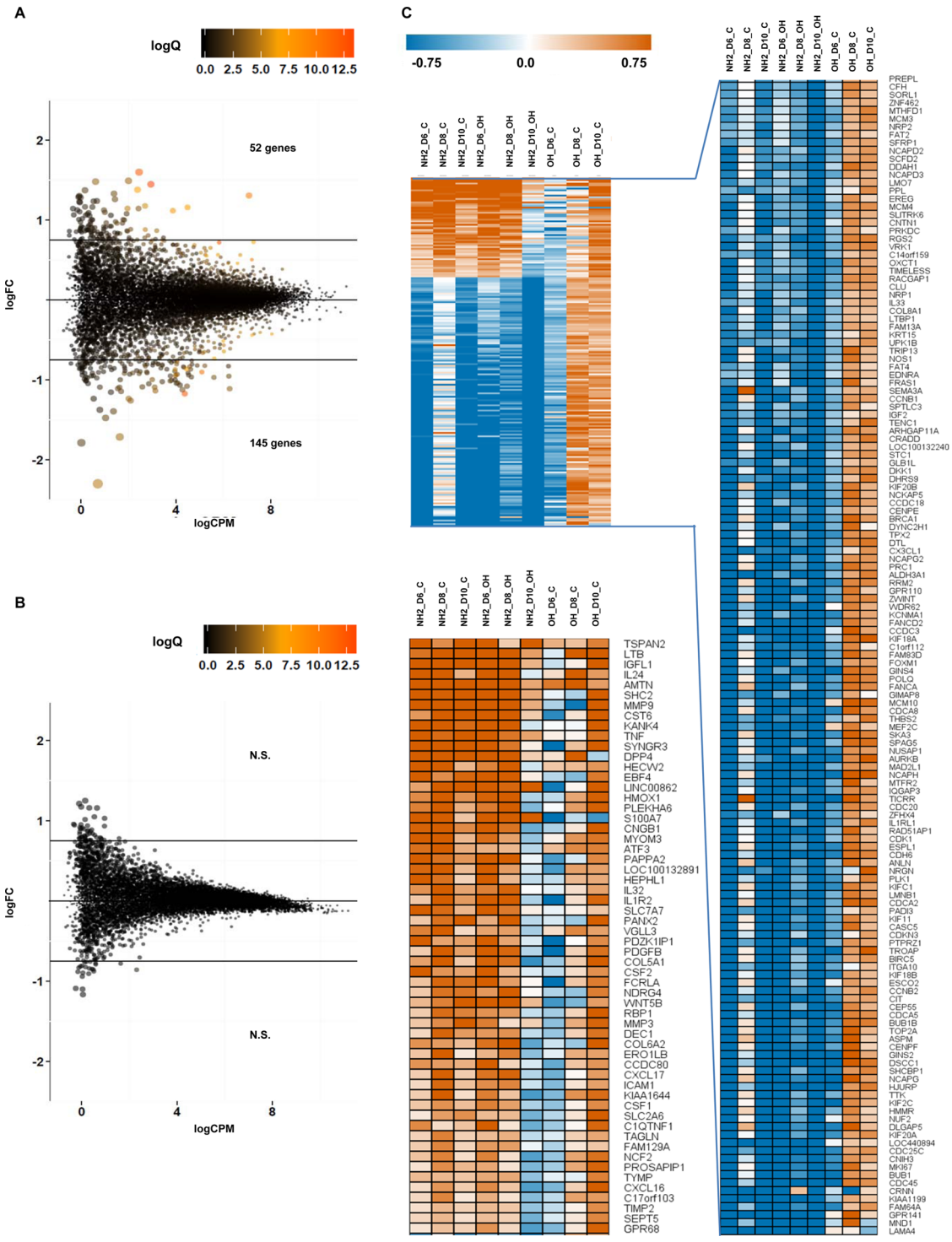

Figure 3. RNA Seq reveals transcriptional changes in primary bronchial epithelial cells exposed to PAMAM-NH_2, but not to PAMAM-OH, at noncytotoxic doses. PBECs from three individual donors were exposed to 0.1 μM PAMAM dendrimers, and samples were subjected to RNA Seq (A) PAMAM-NH_2 *vs* control. The number of genes passing the $q < 0.05$ threshold and filtering is indicated. Log 10 of the multiple-testing corrected *q*-value (logQ) is shown. (B) PAMAM-OH *vs* control; no changes in gene expression were observed. Log 10 of the multiple-testing corrected *q*-value (logQ) is shown. (C) Heat map of the expression changes of genes following exposure to PAMAMs. Only genes that were differentially expressed between PAMAM-NH_2 and control as well as PAMAM-NH_2 and PAMAM-OH are shown. A total of 58 up-regulated and 145 down-regulated genes remained. Donor-specific effect log 2 ratios were calculated by normalizing filtered counts, offsetting the normalized pseudocounts by 0.5 and log 2 transforming them. D, donor.

WNT signaling is activated during lung tissue damage and inflammation, and recent studies have shown that cigarette smoking has adverse effects on members of the WNT family in airway epithelium, promoting a feed-forward mechanism that increases cytokine production by epithelial cells, which could explain why smoking

leads to persistent airway inflammation.[35] Chemokines and growth factors, including CXCL16 and PDGFB (platelet-derived growth factor-β), which promotes the growth especially of cells of mesenchymal origin, such as fibroblasts,[36] were also among the affected genes, along with genes coding for the pro-inflammatory cytokines interleukin (IL)-1β, IL-32 (a protein that induces the production of TNF-α by macrophages), TNF-α, and lymphotoxin β (LTB), a protein with properties very similar to TNF-α. The up-regulation in PBECs of genes involved in immune responses, matrix disassembly, and cell migration is relevant when considering the important immune and barrier function of these cells.

To (partially) validate this approach, we selected one of the up-regulated genes, matrix metalloproteinase 9, or MMP9, as this is a functionally relevant gene and also a transcriptional target of NF-κB (see below), and evaluated MMP9 production in PBECs exposed to PAMAMs. To this end, cells were exposed for 48 h to 0.1 μM PAMAM-OH and PAMAM-NH_2 (*i.e.*, the same conditions as for the RNA Seq analysis), and supernatants were then harvested for analysis of MMP9 expression using ELISA. We found that PAMAM-NH_2, but not PAMAM-OH, induced a 6-fold increase in the secretion of MMP9 (Figure S6B). TNF-α served as a positive control.

Upstream Regulator Analysis Identifies Potential Transcriptional Regulators. We then analyzed the transcriptomics data using the Ingenuity Pathway Analysis software to identify upstream transcriptional regulators that could explain the observed gene expression changes.[37] This analysis implicated the involvement of 16 regulators having an activation Z-score greater than 2 SD units above mean, of which 10 were predicted to be activated and six were predicted to be inhibited. Only regulators that were observed in the RNA sequencing data to be transcribed in PBECs above the level of 1 cpm were included for further consideration. The overlap *p*-values, which measure whether there is a statistically significant overlap between the genes annotated to the regulator in the IPA knowledge database and the list of genes generated by RNA sequencing, ranged between 3.73×10^{-3} and 4.63×10^{-26} (Table S4). Differentially expressed genes in our data set annotated to most regulators included both up- and down-regulated targets. Notably, each of the top-10 regulators were connected almost exclusively to down-regulated genes, and these regulators are mostly well-known factors associated with cell-cycle-related processes and DNA damage responses. Activated regulators, which are predicted to repress their targets, included TP53, NUPR1, RB1, CDKN2A, TCF3, KDM5B, and SMARCB1. Repressed regulators with mainly down-regulated predicted target genes included FOXM1, MYC, FOXO1, E2F1, MYBL2, and HSF1. Using the IPA software, regulator-induced target networks were then generated to study the relationships of the regulators to their targets and to each other (Figure 4A). p53-associated targets accounted for 46/152 down-regulated genes, and 25/46 of these were also associated with the GO category "cell cycle". p53 is accordingly predicted to regulate BUB1, MKI67, and the mitotic kinesin molecular motor protein KIF20A required for chromosome passenger complex (CPC)-mediated cytokinesis.[38] p53 is also predicted to target the cell-cycle-regulated mitotic phosphoprotein DLGAP5 (also known as HURP, for hepatoma up-regulated protein), HMMR (hyaluronan-mediated motility receptor), which forms a complex with BRCA1 and BRCA2, and the cytokinesis-associated motor protein KIF2C, which constitutes the major microtubule plus-end depolymerizing activity in mitotic cells.[39]

FOXM1 is a transcription factor that is critical for G1/S transition and essential for mitotic progression.[40] Interestingly, FOXM1 is the only regulator whose expression was observed to be consistently repressed (Table S4). Our analysis of regulator-induced target networks indicated an interaction between NF-κB and several cell-cycle-related genes including FOXM1 (Figure 4B). Penzo *et al.*[41] have demonstrated that FOXM1 is repressed by sustained NF-κB activation, and molecular analysis in immortalized fibroblasts revealed transient, concerted repression of essential cell cycle effectors that are known targets of either E2F or FOXM1. Moreover, the NF-κB-mediated proliferation arrest was associated with a G1/S phase block in immortalized fibroblasts. Our analysis also disclosed that regulators involved in promoting gene expression that are *activated* mainly included factors associated with the NF-κB-related complex that is involved in and mediates innate immune responses (Figure 4C). These regulators include RELA, ETS1, and ETS2. NFKB1 and NFKBIA do not have a strong significant activation score in the Ingenuity analysis because their predicted targets are discordant with respect to activating and inhibitory roles. The NFKBIA gene, predicted to be inactivated based on the analysis of the gene expression data, encodes a member of the NF-κB inhibitor family. It interacts with REL dimers to inhibit NF-κB/REL complexes that are involved in inflammatory responses.[42] It is noted that while NF-κB can have dual regulatory roles in repressing and activating target genes, the Ingenuity analysis predicts mainly activator roles for genes observed to be regulated in this study.

PAMAM-NH_2 Trigger Cell Cycle Arrest in Human Bronchial Epithelial Cells. Since GO analysis of the RNA Seq data suggested that the genes that were affected primarily represented the cell cycle category, we therefore evaluated the cell cycle in PBECs exposed to PAMAM-OH and PAMAM-NH_2. Remarkably, low-dose exposure of cells to cationic PAMAMs, but not to PAMAM-OH, for 48 h triggered cell cycle arrest. The data show that PAMAM-NH_2 specifically impaired cell cycle progression, with retention of the cells in S-phase (Figure 5A,B).

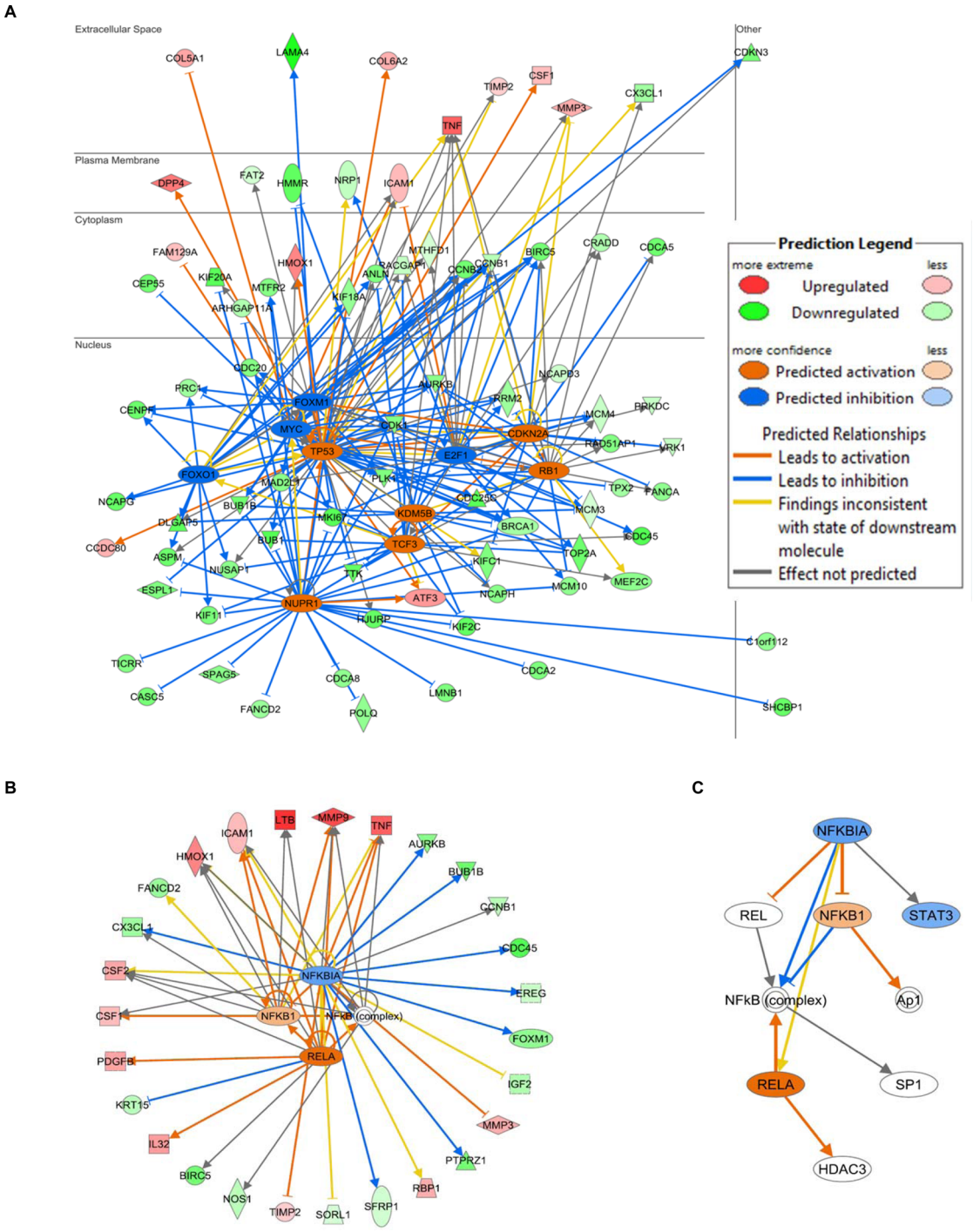

Figure 4. Upstream regulator analysis using the Ingenuity Pathway Analysis (IPA) tool. (A) Transcriptional regulation network around the top-10 upstream regulators by *p*-value, which also have activation Z-score >2 SD (TP53, NUPR1, FOXM1, KDM5B, E2F1, RB1, CDKN2A, FOXO1, MYC, TCF3) (see Table S4 for further information). (B) Upstream regulator analysis indicates modulation of NF-κB and its targets (NF-κB complex, NFKB1, NFKBIA, RELA). (C) Relationships between NF-κB-associated factors, as inferred from PAMAM-NH_2-regulated genes.

With this functional assay we were thus able to corroborate the RNA Seq-based predictions. We also investigated whether higher doses of PAMAM-OH could lead to cell cycle arrest; however, even when PBECs were exposed to higher doses or for a longer period of time, the cell cycle was not affected (Figure 6A–C). The upstream regulator analysis indicated that several of the affected genes, including those related to the cell cycle, were targets of, or linked to, NF-κB activation. Therefore, we evaluated the role of NF-κB activation. To this end, cells were preincubated with a noncytotoxic dose of Bay-117082 (5 μM), a commonly used inhibitor of NF-κB.[43] Our data showed that Bay-117082 completely restored cell cycle progression in PBECs exposed to

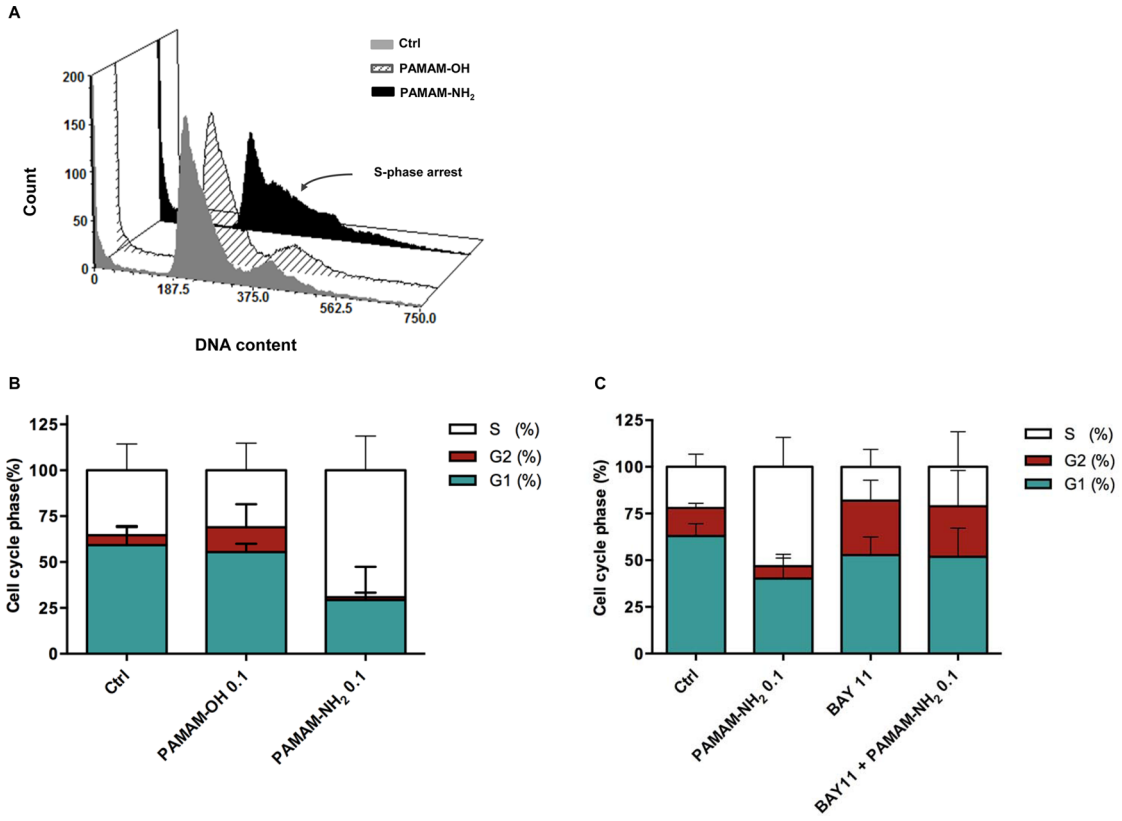

Figure 5. Cationic PAMAMs trigger cell cycle arrest in primary bronchial epithelial cells. PBECs were exposed to 0.1 μM PAMAMs for 48 h. Cell cycle analysis was performed using flow cytometry. (A) Representative histogram. (B) Distribution in each phase of the cell cycle. Note that G2 and M phases are combined. (C) PBECs were exposed to 0.1 μM PAMAMs for 48 h in the presence or absence of the NF-κB inhibitor Bay-117082 (5 μM) followed by cell cycle analysis. The data shown are derived from 3 to 6 independent experiments using three different human donors ($p < 0.05$ Ctrl *vs* PAMAM-NH$_2$ 0.1 μM).**

PAMAM-NH$_2$ (Figure 5C). Moreover, we studied the activation of NF-κB in cells by monitoring the phosphorylation of NF-κB p65 at Ser536 by ELISA and found that exposure of PBECs for 2 h to 0.1 μM PAMAM-NH$_2$, but not PAMAM-OH, resulted in an increase in NF-κB activation by approximately 25% (Figure S6A). TNF-α was used as a positive control. Together, these data support the *in silico* prediction regarding NF-κB as a key determinant of cellular outcomes in this model.

Next, we assessed whether PAMAMs could induce DNA damage, a known trigger of cell cycle arrest, at early (4 h) or late (24 h) time-points, using the comet assay. However, neither PAMAM-OH nor PAMAM-NH$_2$ triggered DNA damage in PBECs at low doses (0.1 μM), while PAMAM-NH$_2$ was shown to induce significant, time-dependent DNA damage at higher doses (1.0 μM) (Figure S7A,B). Hydrogen peroxide was included as a positive control. This suggests that DNA damage is not involved in the low-dose effects of cationic PAMAMs in this model system. In line with this conclusion, we did not detect any effect of the p53 inhibitor pifithrin-α[44] on cell cycle arrest induced by PAMAM-NH$_2$ (not shown). Additionally, the antioxidant catalase also failed to suppress the cell cycle arrest in PAMAM-NH$_2$-exposed PBECs (not shown).

We also evaluated whether low doses of PAMAM-NH$_2$ are able to induce cell cycle arrest in the human lung adenocarcinoma epithelial cell line A549. The A549 cell line was first initiated more than four decades ago from an explanted lung carcinoma and is widely used as a model of the lung epithelium. First, we evaluated cell viability of A549 cells exposed to PAMAMs for 24 and 48 h using the LDH assay. Cell viability was affected only upon exposure to PAMAM-NH$_2$ in a dose- and time-dependent manner and not to PAMAM-OH (Figure 7A–D), but the cells were markedly less sensitive than the primary bronchial epithelial cells. Then, a noncytotoxic dose (1 μM) was selected to evaluate potential effects of PAMAMs on cell cycle progression upon exposure for 48 and 72 h. However, we did not observe any cell cycle arrest in A549 cells following exposure to PAMAMs (Figure 7E). Resveratrol is a compound known to trigger accumulation of cells in S-phase of the cell cycle.[45] As seen in Figure 7F, resveratrol triggered retention of A549 cells in S-phase, showing that these cells are not resistant *per se* to cell cycle arrest.

Senescence Gene Signatures in Human Bronchial Epithelial Cells. Finally, we asked whether PBECs exposed to PAMAM-NH$_2$ dendrimers would eventually recover, or whether these cells would undergo senescence,

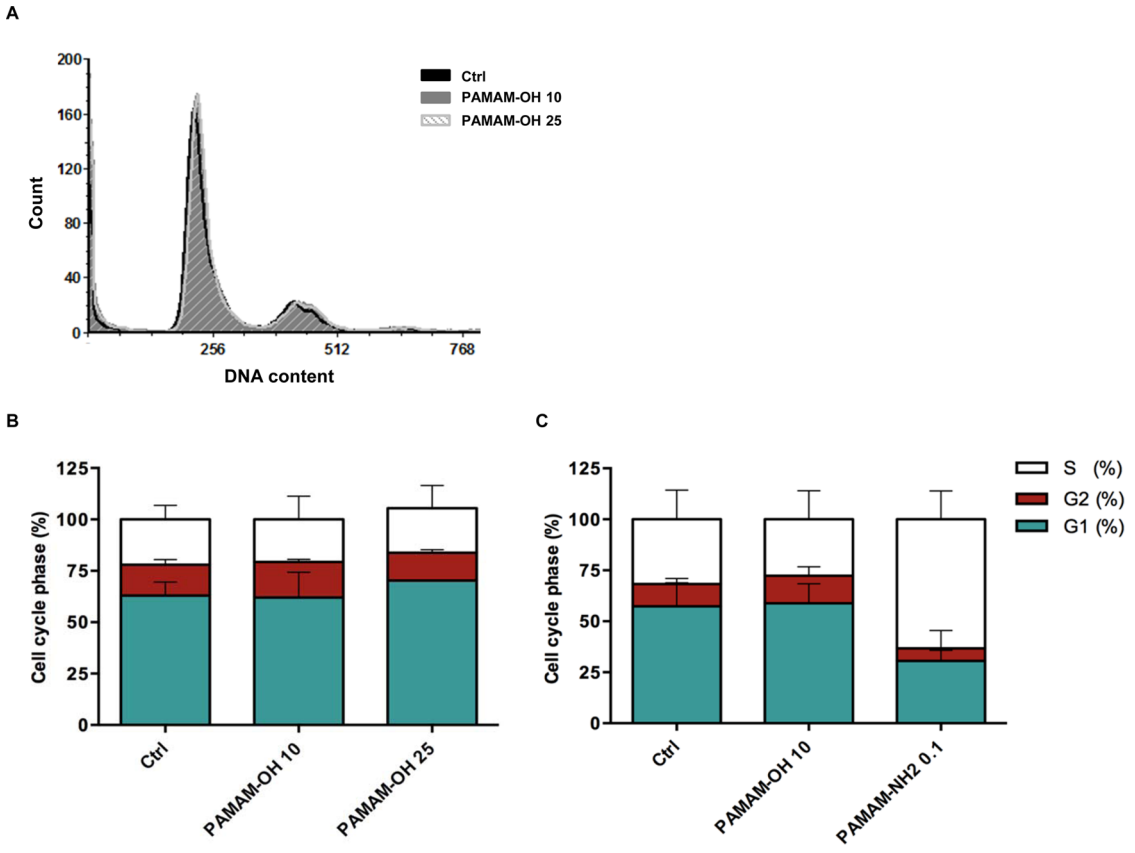

Figure 6. PAMAM-OH dendrimers do not trigger cell cycle arrest in bronchial epithelial cells. PBECs were exposed to PAMAM-OH at 10 or 25 μM for 48 h. Cell cycle analysis was performed using flow cytometry. (A) Representative histogram, with no alterations in cell cycle progression upon exposure to PAMAM-OH. (B) Cell cycle distribution in each phase of the cell cycle. (C) PBECs were exposed to PAMAM-OH (10 μM) or PAMAM-NH_2 (0.1 μM) for 72 h. Data shown are mean values $\pm$ SD from 2 to 3 independent donors.

a "permanent" state of cell cycle arrest. To address this, we performed follow-up experiments in which PBECs exposed to PAMAMs for 48 h as before (0.1 μM) were monitored every 48 h up to 6 days (*i.e.*, 48 h + 48 h + 48 h) (the cells were washed and reseeded in a new plate every 48 h). Cells were then analyzed for cell cycle arrest as before, while senescence was scored by β-galactosidase staining. The experiments confirmed that PAMAM-NH_2 triggered cell cycle arrest in PBECs; furthermore, the results suggested that the cells remained in S-phase arrest also at the 48 h postexposure time-point (Figure S8), but that the cell cycle arrest appeared to be alleviated at 96 h postexposure (not shown). The β-galactosidase staining suggested an increase in senescence after 48 h following exposure to both PAMAMs, as well as during the postexposure phase, but this increase was not statistically significant (Figure S9A–C). Nonetheless, given these results, we interrogated our RNA Seq data and noted a significant overlap between the differentially expressed genes in PAMAM-NH_2-exposed cells and several previously published senescence-specific gene signatures[46–48] (Figure S9D).

DISCUSSION

Using next-generation sequencing and computational approaches, we showed herein that cationic PAMAM dendrimers (PAMAM-NH_2) cause changes in gene expression in primary human bronchial epithelial cells and that gene categories related to cell division and cell cycle were among the most significantly affected categories. Further bioinformatics analyses to identify transcription factors that could explain the observed gene expression changes implicated NF-κB as a putative transcriptional regulator, and functional assays confirmed that the cationic nanoparticles caused cell cycle arrest in PBECs and that this was likely to be mediated *via* NF-κB. We were also able to demonstrate that PBECs exposed to PAMAM-NH_2 dendrimers secreted MMP9, a known downstream target of NF-κB and one of the genes shown to be up-regulated by RNA Seq analysis. We could not, however, confirm a role for p53, another putative upstream regulator, and our cell-based assays showed that low-dose exposure to PAMAMs did not induce DNA damage, a known trigger of p53 activation. Overall, we favor the conclusion that low-dose exposure to cationic PAMAMs leads to NF-κB-dependent cell cycle arrest. We showed that the PAMAMs were taken up by the PBECs through an active, endocytic mechanism and transported to lysosomes. Importantly, PAMAM-NH_2 were more efficiently internalized than PAMAM-OH, suggesting that the transcriptional

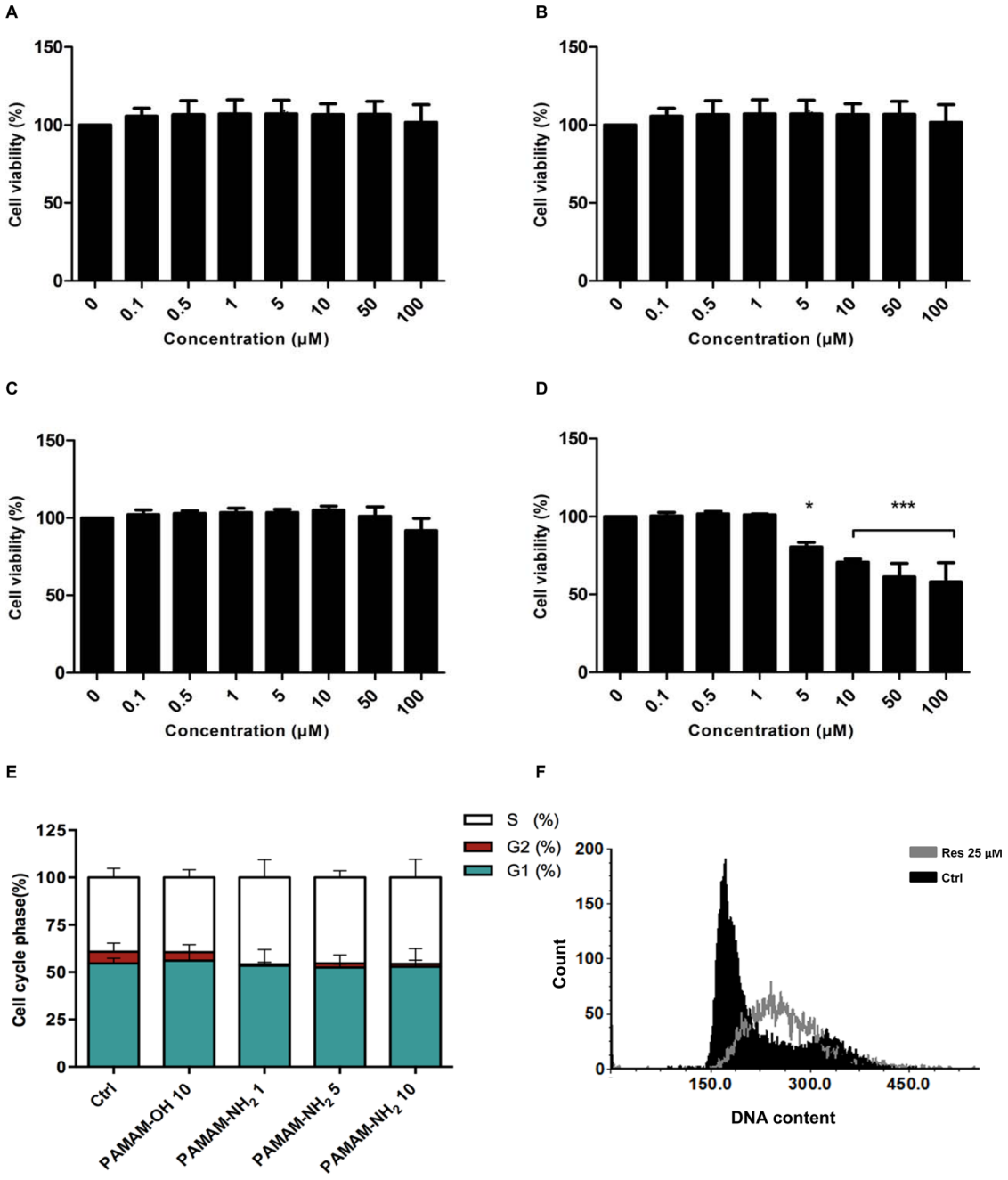

Figure 7. No cell cycle arrest in A549 lung carcinoma cells exposed to PAMAMs. A549 cells were exposed to PAMAM-OH for 24 h (A) and 48 h (C) and to PAMAM-NH_2 for 24 h (B) and 48 h (D), and cell viability was determined using the LDH assay. Results are presented as percent cell viability (mean values ± SD) ($n = 3$). ***$p < 0.001$. (E) Effects of PAMAMs on the cell cycle in A549 cells. Cells were exposed to PAMAM-OH (10 μM) or PAMAM-NH_2 (1, 5, or 10 μM) for 48 h and analyzed using flow cytometry ($n = 3$). (F) Histogram showing cell cycle distribution of A549 cells exposed for 48 h to resveratrol (25 μM), a known inducer of S-phase arrest *vs* control.

changes determined by RNA Seq are correlated with cellular uptake (*i.e.*, intracellular dose) and not with the administered dose.

The issue of dose in nanotoxicology is important. The argument can be made that a majority of *in vitro* studies of nanomaterials are conducted at unrealistically high doses, *i.e.*, unrealistic in relation to the potential human exposure scenario.[23] This may, in turn, have skewed our understanding of nanoparticle effects on biological systems. Indeed, Wang *et al.*[49] reported that chronic, low-dose exposure of human lung epithelial cells to single-walled carbon nanotubes causes malignant transformation with apoptosis resistance, in contradistinction to numerous other studies showing that acute exposure to carbon nanotubes at high doses triggers apoptosis in various cell types.[50] Moreover, Comfort *et al.*[51] showed recently that chronic exposure to very low doses (pg/mL) of silver nanoparticles did not

induce a cytotoxic response, but instead resulted in augmented stress and signaling responses in the human keratinocyte cell line HaCaT. In the present study, we have defined a "low" dose as a dose that does not cause acute cytotoxicity in the cell model in question. Importantly, at this dose—0.1 μM or approximately 1.4 μg/mL—PAMAM-NH_2 dendrimers nonetheless affected numerous genes in bronchial epithelial cells, while PAMAM-OH dendrimers did not affect expression of any genes. This could be due to the fact that the cells internalized the amine-terminated PAMAMs more readily than the hydroxyl-terminated PAMAMs. However, we also found that at higher doses of administered PAMAM-OH dendrimers (10 μM), when the intracellular dose appeared to parallel the dose of internalized PAMAM-NH_2 dendrimers given at a dose of 0.1 μM, as evidenced by our flow cytometric analysis, the PAMAM-OH dendrimers nevertheless failed to trigger cell cycle arrest, suggesting that the surface functional groups play a role not only for cellular uptake but also for the subsequent cellular outcomes. At any rate, we believe that it is important to consider the intracellular dose, not only the administered dose, of nanoparticles. In a recent study, Kodali *et al.*[52] reported that pretreatment of primary murine bone-marrow-derived macrophages with superparamagnetic iron oxide nanoparticles that did not elicit acute cytotoxicity as measured by LDH leakage from these cells caused extensive transcriptional reprogramming in response to bacterial lipopolysaccharide challenge. The authors concluded that biological effects of engineered nanomaterials may not only occur through direct cytotoxicity but be indirectly manifested after challenging normal (immune) cell function. Our present studies using PAMAMs further underscore that low-dose effects of nanoparticles need to be properly investigated. Indeed, bronchial epithelial cells are the first line of defense against inhaled particulates and microorganisms and contribute to apoptotic cell clearance in the airways, which influences airway inflammation in response to common allergens,[53] and the present finding that low-dose exposure of PBECs to cationic PAMAMs caused an up-regulation of genes involved in immune responses, including genes encoding the pro-inflammatory cytokines TNF-α and IL-1β, as well as genes involved in cell migration and disassembly of extracellular matrix, such as MMP3 and MMP9, implies that such nanoparticles could impact innate immune responses in the airways even at doses when innate immune cells (bronchial epithelial cells) are not actually killed.

In an attempt to address the potential long-term consequences of low-dose exposure of PAMAMs, we performed follow-up studies in which cells were monitored for several days following the initial exposure. Interestingly, the results showed that the PBECs remained in cell cycle arrest at 48 h postexposure, but suggested that the cells could gradually recover; at the same time, our gene set enrichment analysis (GSEA) implied that exposure to PAMAM-NH_2 resulted in the induction of genes with significant overlap with senescence-related gene signatures.[46−48] We could not detect a significant increase in senescence using standard techniques; however, it should be noted that during cell cycle arrest caused by contact inhibition, cells do not undergo senescence, thus resuming proliferation after replating.[54] Therefore, the fact that we reseeded our cells every 48 h could potentially have suppressed senescence; on the other hand, not replating the cells would have precluded the long-term (almost 1 week) follow-up of the fate of these cells. Nonetheless, we may conclude with some certainty that PBECs exposed for 48 h to low doses of cationic PAMAM dendrimers display biomarkers/gene signatures of senescence. Further studies are needed to clarify the long-term effects of such exposures.

Several previous studies have shown that exposure to PAMAMs may trigger the production of ROS in mammalian cells as well as in other model organisms.[55−58] In a recent study, Akhtar *et al.*[59] showed that PAMAM-induced stimulation of EGFR-ERK1/2 signaling in human embryonic kidney (HEK 293) cells could be attenuated by antioxidants such as catalase, implying that an oxidative-stress-dependent mechanism was involved. However, in the present study, the administration of catalase to PBECs failed to prevent cell cycle arrest triggered by exposure to low doses of PAMAM-NH_2 dendrimers. Furthermore, we could not detect any ROS production in PBECs exposed to PAMAMs up to 5 h, thus arguing against a role for ROS production as an early signaling event; on the other hand, the increase in ROS levels seen at 48 h may perhaps be interpreted as a consequence of the cellular reactions to PAMAMs, rather than a signaling event that could account for the phenotypic changes (cell cycle arrest). Thus, the exact mechanism linking PAMAM exposure to NF-κB activation and cell cycle arrest awaits further investigation. Bacterial lipopolysaccharides are known to activate NF-κB *via* Toll-like receptors; however, endotoxin contamination was excluded for the PAMAMs used in the present study.

While our gene expression profiling and cell-based assays revealed that the positively charged dendrimers (PAMAM-NH_2) caused down-regulation of genes related to cell division and cell cycle and caused cell cycle arrest in PBECs, we acknowledge that the present study does not allow for generalized structure−activity relationships to be established for nanoparticles. The "predictive" potential of our systems biology approach refers to the fact that we could formulate hypotheses and predict phenotypes based on detailed bioinformatics analysis of the gene expression data and that the mechanistic or phenotypic hypotheses could be validated using targeted experimental studies,

including studies using inhibitors of specific pathways or signaling molecules. Nevertheless, these predictions may not be applicable to other model systems. Indeed, we found that the human lung adenocarcinoma cell line A549 was generally more resistant to the cytotoxic effects of PAMAM-NH_2 and did not display cell cycle arrest when exposed to PAMAM-NH_2, which is unsurprising, as cancer cells commonly harbor defects in cell death and/or cell-cycle-related pathways,[60] and the gene expression profiles of cancer cell lines do not necessarily match those of the tissue of origin.[61] Thus, while others have shown that amino-modified polystyrene nanoparticles (PS-NH_2), but not carboxylated ones (PS-COOH) are capable of interfering with cell cycle progression in A549 cells,[62] these cells did not undergo cell cycle arrest in response to noncytotoxic doses of PAMAM-NH_2. It remains possible that different nanoparticles trigger cell cycle arrest in different cells through different mechanisms. Furthermore, Moos *et al.*[63] performed microarray-based transcriptomic evaluation of human aortic endothelial cell responses exposed to 0.5 μM of generation 4 PAMAM-NH_2 and generation 3.5 PAMAM-COOH and found that the dendrimers did not elicit any detectable transcriptional changes, despite displaying cytotoxicity (PAMAM-NH_2) or no toxicity (PAMAM-COOH). On the other hand, in a recent study of transcriptomic responses in zebrafish embryos, Oliveira *et al.*[64] showed that generation 3 and generation 4 PAMAM-NH_2 caused transcriptional effects at sublethal doses consistent with the activation of the innate immune response. The authors could not detect any markers of oxidative stress following exposure to PAMAMs, but found instead that the dendrimers induced expression of *tnfb*, *irg1l*, *mmp9*, and *mmp13*, genes that are related to the innate immune response to bacteria.[64] The use of fish embryos precludes the identification of the specific tissue and/or cell types participating in the observed responses. Nevertheless, it is interesting to note that similar genes—including MMP9—were up-regulated in the present study. It can thus be speculated that PAMAMs are "sensed" as microbes by immune-competent cells, thereby eliciting a conserved pattern of transcriptional responses.

The present, integrative approach has enabled the discovery of perturbations of categories of genes based on whole transcriptome sequencing through the use of computational tools, followed by confirmation of the systems biology-based predictions using cell-based assays. RNA Seq thus provides new opportunities for global analysis of changes in the expression level of genes in exposed cells,[6] but few studies to date have applied this approach to nanomaterial-exposed cells. It should be noted, however, that next-generation sequencing does not address post-translational modifications, and other complementary approaches, such as (next-generation) proteomics, are therefore needed; in fact, efficient integration of these technologies might ultimately result in "next-generation systems biology".[65] In a recent study, Lucafò *et al.*[66] evaluated the effects of fullerenes in the human MCF-7 breast carcinoma cell line using RNA Seq analysis followed by Connectivity Map analysis to identify similarities between the transcriptional signatures produced by fullerenes and those produced by other compounds with known modes of action. By this approach, the authors could show that the gene expression signature of fullerene-treated cells was strikingly similar to those induced by selective inhibitors of the mammalian target of rapamycin (mTOR) signaling. We also performed CM analysis of our RNA Seq data (see Materials and Methods) and found that the gene expression profile of PAMAM-NH_2 matched the profiles of several other compounds known to cause S-phase arrest (Table S5). In another recent study, Simon *et al.*[67] used RNA Seq approaches to evaluate the effects of exposure to four metal-based nanoparticles, nano-Ag, nano-TiO_2, nano-ZnO, and CdTe/CdS quantum dots (QDs), in the eukaryotic green alga *Chlamydomonas reinhardtii*. Interestingly, nano-TiO_2, nano-ZnO, and QDs elevated the levels of transcripts encoding subunits of the proteasome, which the authors interpreted as a sign of proteasome inhibition. However, whether or not these nanoparticles inhibited the proteasome was not evaluated. Nagy *et al.*[68] employed transcriptome sequencing to gain insight into the cellular responses to quantum dots with different surface functionalization and found that metallothionein genes were up-regulated, which correlated with the leaching of Cd^{2+} ions from the core of the nanoparticles. Additionally, in an instructive example of the use of proteomics and GO-based annotation of omics data, Tsai *et al.*[69] showed that gold nanoparticles can cause cell death through the induction of endoplasmic reticulum (ER) stress in the human myeloid leukemia-derived cell line K562. Taken together, these studies demonstrate how transcriptomic or proteomic profiling can aid in the elucidation of the molecular mechanisms of nanomaterial toxicity.

CONCLUSION

In summary, we present a systems biology approach based on whole transcriptome sequencing coupled with computational methods, including Gene Ontology enrichment analysis and Ingenuity Pathway Analysis, to reveal key pathways involved in cellular responses to engineered nanoparticles. Notably, we have shown that low doses (*i.e.*, doses that do not elicit acute cytotoxicity) of cationic PAMAMs, but not of similar-sized PAMAMs with neutral surface charge, induced specific changes in gene expression, with a pronounced down-regulation of cell-cycle-related genes, of which many were suggested to be targets of NF-κB. Further studies showed that PAMAM-NH_2

exposure leads to cell cycle arrest at low (noncytotoxic) doses, thus corroborating the systems biology-based predictions. We could not demonstrate a role for oxidative stress in this model, nor did we find that PAMAMs triggered DNA damage at low doses. Cell cycle arrest at low-dose exposure to PAMAMs was noted for primary lung cells, but not in lung-derived cancer cells, which therefore are considered a poor model in this particular case. We propose that omics approaches could be used as a tool to identify perturbations of cellular functions in response to nanomaterials, including responses not readily detected by conventional screening approaches, and that such investigations may identify novel end-points of toxicity.

MATERIALS AND METHODS

Nanomaterials. Generation 4 (G4) PAMAM-OH and PAMAM-NH_2 were purchased from Dendritech Inc. (Midland, MI, USA), and fluorescein isothiocyanate (FITC) and 5-(4,6-dichlorotriazinyl) amino fluorescein (5-DTAF) were purchased from (Molecular Probes, Paisley, UK). ZnO nanoparticles (ZincoxTM 10) used as a positive control in cytotoxicity assays were purchased from IBU-tec Advanced Materials AG, Weimar, Germany, and their characterization was reported previously.[22] The size and zeta potential of the PAMAMs are summarized in Table S1.

Fluorescent Labeling. PAMAM-NH_2 and PAMAM-OH were labeled with the fluorescent dyes FITC and 5-DTAF, respectively, according to procedures reported previously.[25,26] The labeled dendrimer solutions were dialyzed against distilled water through sterilized and rinsed membrane tubing (molecular mass cutoff 3.5 kDa) for 24−48 h. Upon subsequent lyophilization, labeled dendrimers were obtained as yellow powders. The material was stored at −20 °C until further use.

Dynamic Light Scattering and Zeta Potential. The experiments were performed on a Malvern Zetasizer NanoZS instrument using a He−Ne laser (Max, 5 mW) at 633 nm. PAMAMs were dispersed in phosphate-buffered saline solution (PBS), deionized water, and keratinocyte serum-free medium, and dynamic light scattering (DLS) and zeta potential were evaluated. Size was determined by triple measurements with 10 scans in each measurement, and averages are reported.

Fourier Transform Infrared Spectroscopy. FT-IR spectroscopy was performed on a PerkinElmer Spectrum 2000 using a MKII Golden Gate, single reflection ATR system. A concentrated droplet of sample was left to dry on the diamond, and spectra were recorded after 15 min, 16 scans per sample.

Endotoxin Assessment. Dendrimers were controlled for endotoxin contamination using the Limulus Amebocyte Lysate (LAL) Endochrome Test (Charles River Endosafe, Charleston, SC, USA) as previously described.[70] The endotoxin content in all PAMAM samples used in the present study was below the FDA-mandated limits of acceptance for chromogenic LAL assays (0.5 EU/mL).

Primary Human Bronchial Epithelial Cells. The establishment of primary bronchial epithelial cells is described in detail in previous publications.[71] Briefly, cells were cultured in 80 cm^2 plastic flasks (Nunc, Roskilde, Denmark) at a density of (1−2) × 10^6 in keratinocyte serum-free medium (KSFM) (Gibco), supplemented with epidermal growth factor (5 ng/mL; Gibco), bovine pituitary extract (50 μg/mL; Gibco), and penicillin/streptomycin (20 U/mL). The cultures were kept at 37 °C in a humidified atmosphere of 5% CO_2 in air, and medium was changed every second day. At confluence the cells were detached by exposure to trypsin/EDTA solution (0.03%/0.01% in calcium- and magnesium-free PBS) and reseeded in 96-well plates at 5.0 × 10^3 cells/well in 24-well plates (Nunc, Roskilde, Denmark) at a concentration of (7.5−10) × 10^3 cells/well or in six-well plates at a concentration of (25−30) × 10^4 cells/well and grown to 80% confluence. The work on PBECs was approved by the ethical review board for human studies at Karolinska Institutet (Forskningsetikkommitte Nord; Dnr 99-357).

A549 Lung Cells. The human lung adenocarcinoma cell line A549 was obtained from the American Type Culture Collection (ATCC) (Manassas, VA, USA) and was maintained in Dulbecco's modified Eagle's medium (DMEM) supplemented with 10% FBS, 1 mM Na-pyruvate, 100 U/mL penicillin, and 100 μg/mL streptomycin (Gibco Invitrogen Corporation) at 37 °C in 5% CO_2.

***In Vitro* Cytotoxicity Assays.** PBECs and A549 cells were incubated in medium alone as negative control or with PAMAMs at the indicated concentrations and time-points. ZnO nanoparticles were included as a positive control. Cell viability was determined using the following methods. LDH assay: Release of lactate dehydrogenase (LDH) from A549 cells and PBECs exposed to PAMAM dendrimers was determined by using the CytoTox 96 nonradioactive cytotoxicity assay (Promega G1780, Madison, WI, USA). Cells were plated in a 96-well plate at the density of 5.0 × 10^4 and 5.0 × 10^5 cells/mL, respectively. Cells were exposed to particles at the doses and time-points indicated. Following exposure, 50 μL of supernatants was assayed for LDH activity following the manufacturer's protocol. Results are expressed as % cytotoxicity = experimental LDH/maximum LDH release, analyzed in triplicates from three or four independent experiments (A549) or using cells from at least three donors (PBECs). Alamar Blue assay: The Alamar Blue assay is used to assess cell viability based on the reduction potential of metabolically active cells. PBECs were seeded in 96-well plates and exposed to the PAMAMs at the concentrations and time-points indicated. After exposure, 10 μL of Alamar Blue reagent (Invitrogen) was added in each well and incubated for 2−4 h at 37 °C. The fluorescence was measured at 560 nm excitation and 590 nm emission wavelengths using a Tecan Infinite F200 plate reader (Männedorf, Switzerland). Results are expressed as percentage cell viability *vs* control. Experiments were performed at least three times in triplicates for each time-point and concentration.

Assessment of ROS Production. Intracellular ROS were measured by a fluorometric assay using carboxy H_2DCFDA [5-(and-6)-carboxy-2,7-dichloro-dihydroflourescein diacetate)]. In brief, PBECs were seeded at a density of 12 × 10^4 cells/mL in a black 96-well microplate (Nunc, Denmark). PBECs were incubated with the fluorescent probe at 37 °C in the dark for 30 min, then exposed to PAMAMs for the indicated time-points. *tert*-Butyl hydroperoxide (TBHP) was used as a positive control. The fluorescence was quantified using a spectrophotometer (Infinite F200, Tecan, Männedorf, Switzerland). Fluorescence was measured using an excitation of 485 nm and emission of 530 nm. Results are expressed as the amount of fluorescence in % of the control.

Quantification of Cellular Uptake. To study the internalization of PAMAMs, PBECs and A549 cells were exposed to the fluorescently labeled PAMAMs for the indicated time-points. Cells were then washed with PBS and incubated with trypan blue (250 μg/mL) (to quench extracellular fluorescence) for 5 min. Cells were then washed, centrifuged at 800 rpm for 5 min, and washed again. Flow cytometry was performed using a FACScan equipped with a 488 nm argon laser (Becton Dickinson, San Jose, CA, USA) operating with CellQuestPro software (Becton Dickinson).

Colocalization Studies. To monitor cellular internalization of labeled PAMAMs, PBECs were seeded in 24-well plates containing coverslips, allowed to attach for 24 h, and were then incubated in the presence of labeled PAMAMs in KSMF medium for 2, 24, or 48 h at 37 °C. In order to determine the subcellular localization of PAMAMs, PBECs were incubated with labeled PAMAMs as indicated. Thirty minutes before fixation, Lysotracker (1 μM) (Invitrogen) was added. Slides were fixed with 4% formaldehyde and counterstained with 5 μg/mL phalloidin−tetramethylrhodamine isothiocyanate (Sigma). DAPI-containing mounting medium was then added (Vector Laboratories, Burlingame, CA, USA), and slides were visualized in an inverted Nikon ECLIPSE TE2000-S fluorescence microscope (Nikon Corp.,

Tokyo, Japan) or using a ZEISS LSM510META microscope (Carl Zeiss AG, Oberkochen, Germany). For specific labeling of lysosomes, PBECs were seeded in 24-well plates. After 12 h, fluorescently labeled PAMAMs were added, and cells were cultured at 37 °C as indicated. Slides were fixed with 4% paraformaldehyde solution, and blocking was then performed with a 2% BSA−PBS solution. Staining with primary antibodies against LAMP-1 (Santa Cruz Biotechnology, Santa Cruz, CA, USA) was followed by staining with secondary goat anti-mouse Alexa 594-labeled antibodies (Invitrogen). Slides were stained with DAPI and visualized using a ZEISS LSM510META microscope.

Cell Cycle Analysis. PBECs and A549 cells were seeded at a density of 12 and 5.0 × 10^4 cells/mL, respectively, in a 12-well plate and exposed to PAMAMs, with or without the following inhibitors: Bay-117082 (Sigma), pifithrin-α (Sigma), and catalase (Calbiochem). After harvesting and washing twice with cold PBS, the cells were resuspended in 500 μL of Triton X-100 staining buffer (0.1% (v/v) Triton X-100 (Sigma) and 0.1% sodium citrate in PBS) to permeabilize the cells. Then, 5 μL of propidium iodide (1 mg/mL, Sigma) was added, and cells were analyzed by flow cytometry within 30 min on a FACSCalibur (Becton Dickinson) operating with CellQuestPro software. MultiCycle AV (De Novo Software, Los Angeles, CA, USA) was used for cell cycle analysis. For the recovery experiments, PBECs were exposed to PAMAMs for 48 h, then washed three times with PBS and maintained in culture as indicated, in the absence of PAMAMs. The cells were reseeded in new plates before reaching confluence.

DNA Damage. The comet assay was performed as described.[72] In brief, cells were embedded into 0.75% low-melting agarose and lysed with a freshly prepared 1% Triton lysis buffer (pH 10) for 1 h. Alkaline unwinding was then performed for 40 min on ice at dark conditions using 0.3 M NaOH (pH > 13) followed by DNA electrophoresis in the same alkaline solution for 30 min at 29 V. After neutralization and fixation, slides were stained with ethidium bromide and scored using a fluorescence microscope (Leica DMLB, Houston, TX, USA) with Comet assay IV software (Perceptive Instruments, Suffolk, UK). H_2O_2 treatment for 10 min on ice was used as a positive control.

***β*-Galactosidase Staining.** Senescence-associated β-galactosidase (SA-β-gal) staining was performed using PBECs (15 × 10^4) grown in 35 mm culture plates according to the manufacturer's instructions (Senescence Cells Histochemical Staining Kit, Sigma-Aldrich). Briefly, cells were exposed to PAMAMs for 48 h, washed with PBS, and then stained. For the recovery experiments, PBECs were exposed to PAMAMs for 48 h, washed three times with PBS, and then maintained in culture for additional time-periods as indicated, in the absence of PAMAMs.

NF-κB p65 Activation. To study activation of NF-κB, phosphorylation of endogenous NF-κB p65 at Ser536 was detected in cell lysates using the PhosphoTracer NF-κB p65 ELISA kit (Abcam, Europe, Cambridge, UK). To this end, PBECs were cultured in 12-well plates and exposed to 0.1 μM PAMAM dendrimers or 10 ng/mL TNF-α for 2 h. After stimulation, the supernatants were collected and kept at −70 °C until analysis, and the cells were lysed. The concentration of NF-κB p65 was analyzed according to the manufacturer's protocol. In order to normalize the loading protein level, total protein of each well was detected by using the DC protein assay kit (Bio-Rad, Solna, Sweden). The experiments were performed in duplicates with PBECs from two donors. Results are expressed as percent change of the corresponding control.

MMP-9 Expression. The secretion of matrix metalloproteinase 9 was measured with a DuoSet ELISA MMP-9 kit (R&D Systems, Europe, Abingdon, UK). The supernatants from cells exposed to 0.1 μM PAMAMs or 10 ng/mL TNF-α for 48 h were analyzed according to the manufacturer's protocol, and for the duplicate samples, an intra-assay variation of <10% was accepted. The experiments were performed in duplicates with PBECs from two donors. The results are expressed as percent change of the corresponding control, and the detection range was 31.5−2000 pg/mL.

RNA Extraction Protocol. PBECs were exposed to PAMAMs, and total RNA was extracted and purified from the cells using Qiagen RNeasy Mini columns with DNase I treatment (Qiagen, Chatsworth, CA, USA). RNA concentration was determined using a NanoDrop spectrophotometer (NanoDrop Technologies, Wilmington, DE, USA), and the samples were kept at −80 °C until further use.

mRNA Sequencing Data Acquisition and Preprocessing. The mRNA Seq of polyadenylated transcripts from total RNA (samples are purified by poly-A enrichment before library creation using Illumina Tru-seq RNA) was used to profile nanoparticle treated and control samples at the Science for Life Laboratory. Data processing was carried out at SNIC-UPPMAX, Uppsala, Sweden.[73] Samples were multiplexed 9-fold using Illumina standard protocols, clustered on cBot, and sequenced on Hi-seq 2500, in RapidRun mode, according to the manufacturer's instructions. Demultiplexing and conversion was done using CASAVA v1.8.2. The quality scale was Sanger/phred33/Illumina 1.8+. Mapping of the reads to a genomic template was done with Tophat/1.3.3, and duplicates were removed with picard-tools/1.29. The raw read counts (the number of sequences that map to each gene/transcript) were calculated using the HT-seq 0.5.1 software and used in the statistical analysis. FPKM values (*i.e.*, fragments per kilobase of transcript per million mapped reads) were additionally calculated using the cufflinks/1.3.0 program using ENSEMBL annotation of genes and transcripts for each sample. Gene expression data were visualized with heat maps using the Multi Experiment Viewer software, version 4.8.1, with genes ordered according to average fold change. Donor-specific effect ratios were calculated by normalizing filtered counts, offsetting the normalized pseudocounts by 0.5, and log 2 transforming them. The sequencing data are deposited at ArrayExpress, accession number E-MTAB-2397.

mRNA Sequencing Data Analysis. Counts, mapped to Ensemble gene identifiers (hg19), from RNA sequencing were processed and further analyzed using the R statistical programming language version 3.0.2 (2013-09-25) and Bioconductor version 2.13 packages edgeR_3.4.1 and limma_3.18.4.[28,29] The counts were annotated with Entrez gene identifiers and gene symbols using the org.Hs.eg.db_2.10.1 package. Counts were initially filtered to remove genes that have less than 1 count per million in at least three samples, as determined by the edgeR function cpm, and then formatted as a DGEList object. The calcNormFactors function was used for determining the relative abundances of tags from each sample. An MDS plot of the tags indicated clustering according to the sample donor, which was taken into account in the modeling of the data for differential gene expression analysis by using a paired design. Differential tag abundance was determined using the edgeR Cox-Reid estimator and the empirical Bayes estimate of the negative binomial dispersion with expression levels specified by a log-linear model using the glmFit function. Gene-wise statistical tests were conducted using contrasts between treatments and controls with glmLRT function and Benjamini-Hochberg multiple testing correction at $q < 0.05$. Only genes that were differentially expressed between PAMAM-NH_2 and control as well as PAMAM-NH_2 and PAMAM-OH were further analyzed. In addition donor-specific effect ratios were calculated by normalizing filtered counts, offsetting the normalized pseudocounts by 0.5 and log 2 transforming them. Genes were filtered by requiring that from the PAMAM-NH_2 *vs* controls and *vs* PAMAM-OH ratios 5/6 had to be in in the same direction.

Gene Ontology Enrichment Analysis. Gene Ontology enrichment analysis was performed with R/Bioconductor package topGO_2.14.0 using gene ontology annotations from GO.db_2.10.1 and org.Hs.eg.db_2.10.1.[74] After filtering out genes without Entrez identifiers, a total of 58 up-regulated and 145 down-regulated genes remained. GO enrichment analysis was performed with the Fisher's exact test and the weight01 test statistic for eliminating local similarities and dependencies between GO terms. Only categories that had a significance of $p < 0.01$ and at least three significant genes are reported.

Pathway and Upstream Regulator Analysis. Ingenuity Pathway Analysis (application version 220217, content version 16542223) (license obtained from Ingenuity Systems, Redwood City, CA, USA) was performed in order to interpret the mRNA sequencing data. Both canonical pathway enrichment analysis and upstream regulator analysis were performed. We used as a cutoff $p < 0.01$

and the overlap of at least three significantly effected genes. In addition regulators were filtered by activation Z-score, and all regulators were required to be expressed at least at a level of 1 count per million in at least three biological replicates.

Senescence-Associated Gene Signatures. To evaluate whether PAMAMs induced senescence-associated genes, the rotation gene set testing for linear models (mroast)[75] in limma version 3.20.1 was used to test the significance of four distinct senescence-associated gene signatures extracted from the literature.[46−48] Counts summarized to Ensembl gene models were used for analysis, and only genes with 1 count per million or more in at least three biological replicates were analyzed. To improve the specificity of the analysis, duplicate genes/transcripts were removed, selecting the models with the most counts for each gene. Using the R/Bioconductor edgeR package version 3.6.1,[76] a robust estimate of the negative binomial dispersion parameter for each tag or transcript was computed.[77] A pairwise linear model was fitted taking into account donor variation. Statistical significance of each signature was evaluated using the mean50 method with 19 998 rotations, and the nondirectional false discovery rate was taken as a measure of significance.

Connectivity Map Analysis. The list of up- and down-regulated genes in response to exposure to PAMAM-NH_2 dendrimers was converted into Affymetrix HG-U133A identifiers to allow the comparison with microarray-based expression data. The gene sets were subjected to Connectivity Map analysis[17] to identify similarities between the transcriptional signatures produced by PAMAM-NH_2 and those produced by other perturbagens. Significant connection was concluded at a p-value of <0.01.

Statistical Analysis. Differences between groups were evaluated using ANOVA followed by Tukey's *post hoc* test using GraphPad Prism version 5.02 for Windows (GraphPad Software, San Diego, CA, USA). The level of significance for rejecting the null hypothesis of zero treatment effect was $p = 0.05$.

Conflict of Interest: The authors declare no competing financial interest.

Acknowledgment. This work was supported by the Swedish Cancer and Allergy Foundation, Swedish Research Council, and the Seventh Framework Programme of the European Commission (FP7-NANOMMUNE-Grant Agreement No. 214281; FP7-NANOSOLUTIONS-Grant Agreement No. 309329). We thank the Science for Life Laboratory for RNA sequencing and L. Valero (Université Paris Descartes and Karolinska Institutet) for assistance with senescence analysis. P. Gerde (Karolinska Institutet) is acknowledged for useful discussions on dosimetry.

Supporting Information Available: Supplementary Tables 1−5 and Supplementary Figures 1−9 with figure legends. This material is available free of charge *via* the Internet at http://pubs.acs.org

REFERENCES AND NOTES

1. Kim, B. Y.; Rutka, J. T.; Chan, W. C. Nanomedicine. *N. Engl. J. Med.* **2010**, *363*, 2434–2443.
2. Albanese, A.; Tang, P. S.; Chan, W. C. The Effect of Nanoparticle Size, Shape, and Surface Chemistry on Biological Systems. *Annu. Rev. Biomed. Eng.* **2012**, *14*, 1–16.
3. Fadeel, B.; Feliu, N.; Vogt, C.; Abdelmonem, A. M.; Parak, W. J. Bridge over Troubled Waters: Understanding the Synthetic and Biological Identities of Engineered Nanomaterials. *Wiley Interdiscip. Rev. Nanomed. Nanobiotechnol.* **2013**, *5*, 111–129.
4. Zhu, M.; Zhu, M.; Nie, G.; Meng, H.; Xia, T.; Nel, A.; Zhao, Y. Physicochemical Properties Determine Nanomaterial Cellular Uptake, Transport, and Fate. *Acc. Chem. Res.* **2013**, *46*, 622–631.
5. Klaper, R.; Arndt, D.; Bozich, J.; Dominguez, G. Molecular Interactions of Nanomaterials and Organisms: Defining Biomarkers for Toxicity and High-Throughput Screening using Traditional and Next-Generation Sequencing Approaches. *Analyst* **2014**, *139*, 882–895.
6. Wang, Z.; Gerstein, M.; Snyder, M. RNA-Seq: A Revolutionary Tool for Transcriptomics. *Nat. Rev. Genet.* **2009**, *10*, 57–63.
7. Chen, M.; Zhang, M.; Borlak, J.; Tong, W. A Decade of Toxicogenomic Research and Its Contribution to Toxicological Science. *Toxicol. Sci.* **2012**, *130*, 217–228.
8. Krewski, D.; Westphal, M.; Al-Zoughool, M.; Croteau, M. C.; Andersen, M. E. New Directions in Toxicity Testing. *Annu. Rev. Public Health* **2011**, *32*, 161–178.
9. Collins, F. S.; Gray, G. M.; Bucher, J. R. Toxicology. Transforming Environmental Health Protection. *Science* **2008**, *319*, 906–907.
10. Nel, A.; Xia, T.; Meng, H.; Wang, X.; Lin, S.; Ji, Z.; Zhang, H. Nanomaterial Toxicity Testing in the 21st Century: Use of a Predictive Toxicological Approach and High-Throughput Screening. *Acc. Chem. Res.* **2012**, *46*, 607–621.
11. Hanagata, N.; Zhuang, F.; Connolly, S.; Li, J.; Ogawa, N.; Xu, M. Molecular Responses of Human Lung Epithelial Cells to the Toxicity of Copper Oxide Nanoparticles Inferred from Whole Genome Expression Analysis. *ACS Nano* **2011**, *5*, 9326–9338.
12. Foldbjerg, R.; Irving, E. S.; Hayashi, Y.; Sutherland, D. S.; Thorsen, K.; Autrup, H.; Beer, C. Global Gene Expression Profiling of Human Lung Epithelial Cells after Exposure to Nanosilver. *Toxicol. Sci.* **2012**, *130*, 145–157.
13. Shim, W.; Paik, M. J.; Nguyen, D. T.; Lee, J. K.; Lee, Y.; Kim, J. H.; Shin, E. H.; Kang, J. S.; Jung, H. S.; Choi, S.; *et al*. Analysis of Changes in Gene Expression and Metabolic Profiles Induced by Silica-Coated Magnetic Nanoparticles. *ACS Nano* **2012**, *6*, 7665–7680.
14. Tuomela, S.; Autio, R.; Buerki-Thurnherr, T.; Arslan, O.; Kunzmann, A.; Andersson-Willman, B.; Wick, P.; Mathur, S.; Scheynius, A.; Krug, H. F.; *et al*. Gene Expression Profiling of Immune-Competent Human Cells Exposed to Engineered Zinc Oxide or Titanium Dioxide Nanoparticles. *PLoS One* **2013**, *8*, e68415.
15. Li, X.; He, Q.; Shi, J. Global Gene Expression Analysis of Cellular Death Mechanisms Induced by Mesoporous Silica Nanoparticle-Based Drug Delivery System. *ACS Nano* **2014**, *8*, 1309–1320.
16. McQuillan, J. S.; Shaw, A. M. Differential Gene Regulation in the Ag Nanoparticle and Ag^+-Induced Silver Stress Response in *Escherichia coli*: A Full Transcriptomic Profile. *Nanotoxicology* **2014**, *8* (Suppl 1), 177–84.
17. Lamb, J.; Crawford, E. D.; Peck, D.; Modell, J. W.; Blat, I. C.; Wrobel, M. J.; Lerner, J.; Brunet, J. P.; Subramanian, A.; Ross, K. N.; *et al*. The Connectivity Map: Using Gene-Expression Signatures to Connect Small Molecules, Genes, and Disease. *Science* **2006**, *313*, 1929–1935.
18. Menjoge, A. R.; Kannan, R. M.; Tomalia, D. A. Dendrimer-Based Drug and Imaging Conjugates: Design Considerations for Nanomedical Applications. *Drug Discovery Today* **2010**, *15*, 171–185.
19. Dobrovolskaia, M. A.; Patri, A.; Simak, J.; Hall, J.; Semberova, J.; de Paoli Lacerda, S. Nanoparticle Size and Surface Charge Determine Effects of PAMAM Dendrimers on Human Platelets *in Vitro*. *Mol. Pharmaceutics* **2012**, *9*, 382–393.
20. Albertazzi, L.; Gherardini, L.; Brondi, M.; Sulis Sato, S.; Bifone, A.; Pizzorusso, T.; Ratto, G. M.; Bardi, G. *In Vivo* Distribution and Toxicity of PAMAM Dendrimers in the Central Nervous System Depend on their Surface Chemistry. *Mol. Pharmacol.* **2012**, *10*, 249–260.
21. Lambrecht, B. N.; Hammad, H. The Airway Epithelium in Asthma. *Nat. Med.* **2012**, *18*, 684–692.
22. Shi, J.; Karlsson, H. L.; Johansson, K.; Gogvadze, V.; Xiao, L.; Li, J.; Burks, T.; Garcia-Bennett, A.; Uheida, A.; Muhammed, M.; *et al*. Microsomal Glutathione Transferase 1 Protects against Toxicity Induced by Silica Nanoparticles but Not by Zinc Oxide Nanoparticles. *ACS Nano* **2012**, *6*, 1925–1938.
23. Oberdörster, G. Safety Assessment for Nanotechnology and Nanomedicine: Concepts of Nanotoxicology. *J. Int. Med.* **2010**, *267*, 89–105.
24. Perumal, O. P.; Inapagolla, R.; Kannan, S.; Kannan, R. M. The Effect of Surface Functionality on Cellular Trafficking of Dendrimers. *Biomaterials* **2008**, *29*, 3469–3476.

25. Yu, K.; Russo, P. S. Light Scattering and Fluorescence Photobleaching Recovery Study of Poly(Amidoamine) Cascade Polymers in Aqueous Solution. *J. Polym. Sci., Part B: Polym. Phys.* **1996**, *34*, 1467–1475.
26. Kannan, S.; Kolhe, P.; Raykova, V.; Glibatec, M.; Kannan, R. M.; Lieh-Lai, M.; Bassett, D. Dynamics of Cellular Entry and Drug Delivery by Dendritic Polymers into Human Lung Epithelial Carcinoma Cells. *J. Biomat. Sci., Polym. E* **2004**, *15*, 311–330.
27. Albertazzi, L.; Serresi, M.; Albanese, A.; Beltram, F. Dendrimer Internalization and Intracellular Trafficking in Living Cells. *Mol. Pharmaceutics* **2010**, *7*, 680–688.
28. Anders, S.; McCarthy, D. J.; Chen, Y.; Okoniewski, M.; Smyth, G. K.; Huber, W.; Robinson, M. D. Count-Based Differential Expression Analysis of RNA Sequencing Data Using R and Bioconductor. *Nat. Protoc.* **2013**, *8*, 1765–1786.
29. Robinson, M. D.; McCarthy, D. J.; Smyth, G. K. edgeR: A Bioconductor Package for Differential Expression Analysis of Digital Gene Expression Data. *Bioinformatics* **2010**, *26*, 139–140.
30. Costa, A.; Hood, I. B.; Berger, J. M. Mechanisms for Initiating DNA Replication in Cells. *Annu. Rev. Biochem.* **2013**, *82*, 25–54.
31. Sadasivam, S.; DeCaprio, J. A. The DREAM Complex: Master Coordinator of Cell Cycle-Dependent Gene Expression. *Nat. Rev. Cancer* **2013**, *13*, 585–595.
32. Narlikar, G. J.; Sundaramoorthy, R.; Owen-Hughes, T. Mechanisms and Functions of ATP-Dependent Chromatin-Remodeling Enzymes. *Cell* **2013**, *154*, 490–503.
33. Altieri, D. C. Survivin, Cancer Networks and Pathway-Directed Drug Discovery. *Nat. Rev. Cancer* **2008**, *8*, 61–70.
34. Khokha, R.; Murthy, A.; Weiss, A. Metalloproteinases and Their Natural Inhibitors in Inflammation and Immunity. *Nat. Rev. Immunol.* **2013**, *13*, 649–665.
35. Heijink, I. H.; de Bruin, H. G.; van den Berge, M.; Bennink, L. J.; Brandenburg, S. M.; Gosens, R.; van Oosterhout, A. J.; Postma, D. S. Role of Aberrant WNT Signalling in the Airway Epithelial Response to Cigarette Smoke in Chronic Obstructive Pulmonary Disease. *Thorax* **2013**, *68*, 709–716.
36. Andrae, J.; Gallini, R.; Betsholtz, C. Role of Platelet-Derived Growth Factors in Physiology and Medicine. *Genes Dev.* **2008**, *22*, 1276–1312.
37. Krämer, A.; Green, J.; Pollard, J., Jr.; Tugendreich, S. Causal Analysis Approaches in Ingenuity Pathway Analysis. *Bioinformatics* **2014**, *30*, 523–530.
38. Carmena, M.; Wheelock, M.; Funabiki, H.; Earnshaw, W. C. The Chromosomal Passenger Complex (CPC): From Easy Rider to the Godfather of Mitosis. *Nat. Rev. Mol. Cell Biol.* **2012**, *13*, 789–803.
39. Pujana, M. A.; Han, J. D.; Starita, L. M.; Stevens, K. N.; Tewari, M.; Ahn, J. S.; Rennert, G.; Moreno, V.; Kirchhoff, T.; Gold, B.; *et al*. Network Modeling Links Breast Cancer Susceptibility and Centrosome Dysfunction. *Nat. Genet.* **2007**, *39*, 1338–1349.
40. Wang, I. C.; Chen, Y. J.; Hughes, D.; Petrovic, V.; Major, M. L.; Park, H. J.; Tan, Y.; Ackerson, T.; Costa, R. H. Forkhead Box M1 Regulates the Transcriptional Network of Genes Essential for Mitotic Progression and Genes Encoding the SCF (Skp2-Cks1) Ubiquitin Ligase. *Mol. Cell. Biol.* **2005**, *24*, 10875–10894.
41. Penzo, M.; Massa, P. E.; Olivotto, E.; Bianchi, F.; Borzi, R. M.; Hanidu, A.; Li, X.; Li, J.; Marcu, K. B. Sustained NF-κB Activation Produces a Short-Term Cell Proliferation Block in Conjunction with Repressing Effectors of Cell Cycle Progression Controlled by E2F or FoxM1. *J. Cell Physiol.* **2009**, *218*, 215–227.
42. Perkins, N. D. The Diverse and Complex Roles of NF-κB Subunits in Cancer. *Nat. Rev. Cancer* **2012**, *12*, 121–132.
43. Jitkaew, S.; Trebinska, A.; Grzybowska, E.; Carlsson, G.; Nordström, A.; Lehtiö, J.; Fröjmark, A. S.; Dahl, N.; Fadeel, B. N$^{\alpha}$-Tosyl-L-Phenylalanine Chloromethyl Ketone Induces Caspase-Dependent Apoptosis in Transformed Human B Cell Lines with Transcriptional Down-Regulation of Anti-Apoptotic HS1-Associated Protein X-1. *J. Biol. Chem.* **2009**, *284*, 27827–27837.
44. Komarov, P. G.; Komarova, E. A.; Kondratov, R. V.; Christov-Tselkov, K.; Coon, J. S.; Chernov, M. V.; Gudkov, A. V. A Chemical Inhibitor of p53 That Protects Mice from the Side Effects of Cancer Therapy. *Science* **1999**, *285*, 1733–1737.
45. Panayiotidis, M. I.; Rancourt, R. C.; Pappa, A.; White, C. W. Effect of Cell Cycle Growth Arrest on Global DNA Methylation Status in Human Lung Epithelial-Like (A549) Cells. *In Vivo* **2006**, *20*, 861–865.
46. Coppé, J. P.; Patil, C. K.; Rodier, F.; Sun, Y.; Muñoz, D. P.; Goldstein, J.; Nelson, P. S.; Desprez, P. Y.; Campisi, J. Senescence-Associated Secretory Phenotypes Reveal Cell-Nonautonomous Functions of Oncogenic RAS and the p53 Tumor Suppressor. *PLoS Biol.* **2008**, *6*, 2853–2868.
47. Coppola, D.; Balducci, L.; Chen, D. T.; Loboda, A.; Nebozhyn, M.; Staller, A.; Fulp, W. J.; Dalton, W.; Yeatman, T.; Brem, S. Senescence-Associated-Gene Signature Identifies Genes Linked to Age, Prognosis, and Progression of Human Gliomas. *J. Geriatr. Oncol.* **2014**, *5*, 389–399.
48. Lackner, D. H.; Hayashi, M. T.; Cesare, A. J.; Karlseder, J. A Genomics Approach Identifies Senescence-Specific Gene Expression Regulation. *Aging Cell* **2014**, *13*, 946–950.
49. Wang, L.; Luanpitpong, S.; Castranova, V.; Tse, W.; Lu, Y.; Pongrakhananon, V.; Rojanasakul, Y. Carbon Nanotubes Induce Malignant Transformation and Tumorigenesis of Human Lung Epithelial Cells. *Nano Lett.* **2011**, *1*, 2796–2803.
50. Andón, F. T.; Fadeel, B. Programmed Cell Death: Molecular Mechanisms and Implications for Safety Assessment of Nanomaterials. *Acc. Chem. Res.* **2013**, *46*, 733–742.
51. Comfort, K. K.; Braydich-Stolle, L. K.; Maurer, E. I.; Hussain, S. M. Less Is More: Long-Term *in Vitro* Exposure to Low Levels of Silver Nanoparticles Provides New Insights for Nanomaterial Evaluation. *ACS Nano* **2014**, *8*, 3260–3271.
52. Kodali, V.; Littke, M. H.; Tilton, S. C.; Teeguarden, J. G.; Shi, L.; Frevert, C. W.; Wang, W.; Pounds, J. G.; Thrall, B. D. Dysregulation of Macrophage Activation Profiles by Engineered Nanoparticles. *ACS Nano* **2013**, *7*, 6997–7010.
53. Juncadella, I. J.; Kadl, A.; Sharma, A. K.; Shim, Y. M.; Hochreiter-Hufford, A.; Borish, L.; Ravichandran, K. S. Apoptotic Cell Clearance by Bronchial Epithelial Cells Critically Influences Airway Inflammation. *Nature* **2013**, *493*, 547–551.
54. Leontieva, O. V.; Demidenko, Z. N.; Blagosklonny, M. V. Contact Inhibition and High Cell Density Deactivate the Mammalian Target of Rapamycin Pathway, Thus Suppressing the Senescence Program. *Proc. Natl. Acad. Sci. U.S.A.* **2014**, *111*, 8832–8837.
55. Naha, P. C.; Davoren, M.; Lyng, F. M.; Byrne, H. J. Reactive Oxygen Species (ROS) Induced Cytokine Production and Cytotoxicity of PAMAM Dendrimers in J774A.1 Cells. *Toxicol. Appl. Pharmacol.* **2010**, *246*, 91–99.
56. Mukherjee, S. P.; Lyng, F. M.; Garcia, A.; Davoren, M.; Byrne, H. J. Mechanistic Studies of *in Vitro* Cytotoxicity of Poly(Amidoamine) Dendrimers in Mammalian Cells. *Toxicol. Appl. Pharmacol.* **2010**, *248*, 259–268.
57. Santiago-Morales, J.; Rosal, R.; Hernando, M. D.; Ulaszewska, M. M.; García-Calvo, E.; Fernández-Alba, A. R. Fate and Transformation Products of Amine-Terminated PAMAM Dendrimers under Ozonation and Irradiation. *J. Hazard. Mater.* **2014**, *266*, 102–113.
58. Gonzalo, S.; Rodea-Palomares, I.; Leganés, F.; García-Calvo, E.; Rosal, R.; Fernández-Pinas, F. First Evidences of PAMAM Dendrimer Internalization in Microorganisms of Environmental Relevance: A Linkage with Toxicity and Oxidative Stress. *Nanotoxicology* **2014**, Oct 17: 1−13. [Epub ahead of print].
59. Akhtar, S.; Chandrasekhar, B.; Attur, S.; Yousif, M. H.; Benter, I. F. On the Nanotoxicity of PAMAM Dendrimers: Superfect® Stimulates the EGFR-ERK1/2 Signal Transduction Pathway *via* an Oxidative Stress-Dependent Mechanism in HEK 293 Cells. *Int. J. Pharm.* **2013**, *448*, 239–246.
60. Hanahan, D.; Weinberg, R. A. Hallmarks of Cancer: The Next Generation. *Cell* **2011**, *144*, 646–674.
61. Sandberg, R.; Ernberg, I. Assessment of Tumor Characteristic Gene Expression in Cell Lines Using a Tissue Similarity

Index (TSI). *Proc. Natl. Acad. Sci. U.S.A.* **2005**, *102*, 2052–2057.
62. Kim, J. A.; Åberg, C.; de Cárcer, G.; Malumbres, M.; Salvati, A.; Dawson, K. A. Low Dose of Amino-Modified Nanoparticles Induces Cell Cycle Arrest. *ACS Nano* **2013**, *7*, 7483–7494.
63. Moos, P. J.; Honeggar, M.; Malugin, A.; Herd, H.; Thiagarajan, G.; Ghandehari, H. Transcriptional Responses of Human Aortic Endothelial Cells to Nanoconstructs Used in Biomedical Applications. *Mol. Pharmaceutics* **2013**, *10*, 3242–3252.
64. Oliveira, E.; Casado, M.; Faria, M.; Soares, A. M. V. M; Navas, J. M.; Barata, C.; Piña, B. Transcriptomic Response of Zebrafish Embryos to Polyaminoamine (PAMAM) Dendrimers. *Nanotoxicology* **2014**, *8* (Suppl 1), 92–99.
65. Altelaar, A. F.; Munoz, J.; Heck, A. J. Next-Generation Proteomics: Towards an Integrative View of Proteome Dynamics. *Nat. Rev. Genet.* **2013**, *14*, 35–48.
66. Lucafò, M.; Gerdol, M.; Pallavicini, A.; Pacor, S.; Zorzet, S.; Da Ros, T.; Prato, M.; Sava, G. Profiling the Molecular Mechanism of Fullerene Cytotoxicity on Tumor Cells by RNA-Seq. *Toxicology* **2013**, *314*, 183–192.
67. Simon, D. F.; Domingos, R. F.; Hauser, C.; Hutchins, C. M.; Zerges, W.; Wilkinson, K. J. Transcriptome Sequencing (RNA-Seq) Analysis of the Effects of Metal Nanoparticle Exposure on the Transcriptome of *Chlamydomonas reinhardtii*. *Appl. Environ. Microbiol.* **2013**, *79*, 4774–4785.
68. Nagy, A.; Hollingsworth, J. A.; Hu, B.; Steinbrück, A.; Stark, P. C.; Rios, V. C.; Vuyisich, M.; Stewart, M. H.; Atha, D. H.; Nelson, B. C.; *et al*. Functionalization-Dependent Induction of Cellular Survival Pathways by CdSe Quantum Dots in Primary Normal Human Bronchial Epithelial Cells. *ACS Nano* **2013**, *7*, 8397–8411.
69. Tsai, Y. Y.; Huang, Y. H.; Chao, Y. L.; Hu, K. Y.; Chin, L. T.; Chou, S. H.; Hour, A. L.; Yao, Y. D.; Tu, C. S.; Liang, Y. J.; *et al*. Identification of the Nanogold Particle-Induced Endoplasmic Reticulum Stress by Omic Techniques and Systems Biology Analysis. *ACS Nano* **2011**, *5*, 9354–9369.
70. Feliu, N.; Walter, M. V.; Montañez, M. I.; Kunzmann, A.; Hult, A.; Nyström, A.; Malkoch, M.; Fadeel, B. Stability and Biocompatibility of a Library of Polyester Dendrimers in Comparison to Polyamidoamine Dendrimers. *Biomaterials* **2012**, *33*, 1970–1981.
71. Strandberg, K.; Palmberg, L.; Larsson, K. Effect of Formoterol and Salmeterol on IL-6 and IL-8 Release in Airway Epithelial Cells. *Respir. Med.* **2007**, *101*, 1132–1139.
72. Gliga, A. R.; Skoglund, S.; Wallinder, I. O.; Fadeel, B.; Karlsson, H. L. Size-Dependent Cytotoxicity of Silver Nanoparticles in Human Lung Cells: The Role of Cellular Uptake, Agglomeration and Ag Release. *Part. Fibre Toxicol.* **2014**, Feb 17, 11:11.
73. Lampa, S.; Dahlö, M.; Olason, P. I.; Hagberg, J.; Spjuth, O. Lessons Learned from Implementing a National Infrastructure in Sweden for Storage and Analysis of Next-Generation Sequencing Data. *Gigascience* **2013**, *2*, 9.
74. Alexa, A.; Rahnenführer, J.; Lengauer, T. Improved Scoring of Functional Groups from Gene Expression Data by Decorrelating GO Graph Structure. *Bioinformatics* **2006**, *22*, 1600–1607.
75. Wu, D.; Lim, E.; Francois Vaillant, F.; Asselin-Labat, M.-L.; Visvader, J. E.; Smyth, G. K. ROAST: Rotation Gene Set Tests for Complex Microarray Experiments. *Bioinformatics* **2010**, *26*, 2176–2182.
76. McCarthy, D. J.; Chen, Y.; Smyth, G. K. Differential Expression Analysis of Multifactor RNA-Seq Experiments with Respect to Biological Variation. *Nucleic Acids Res.* **2012**, *40*, 4288–4297.
77. Zhou, X.; Lindsay, H.; Robinson, M. D. Robustly Detecting Differential Expression in RNA Sequencing Data Using Observation Weights. *Nucleic Acids Res.* **2014**, *42* (11), e91.